11-10-2017

Prevention of Alkali-Silica Reaction (ASR) in Lightweight Wellbore Cements Containing Silica-Based Microspheres

Dylan Albers
Louisiana State University and Agricultural and Mechanical College, dalber1@lsu.edu

PREVENTION OF ALKALI-SILICA REACTION (ASR) IN LIGHTWEIGHT WELLBORE CEMENTS CONTAINING SILICA-BASED MICROSPHERES

A Thesis

Submitted to the Graduate Faculty of the
Louisiana State University and
Agricultural and Mechanical College
in partial fulfillment of the degree of
Master of Science

in

The Department of Petroleum Engineering

by
Dylan Albers
B.S., Louisiana State University, 2015
December 2017

ACKNOWLEDGEMENTS

I would like to express my sincere thanks to Dr. Mileva Radonjic for her tireless guidance and support throughout the work of this project and beyond. I would also like to thank my committee members Dr. Clayton Loehn, Dr. Karsten Thompson, and Dr. Wei-Hsung Wang as committee members for their input on this project.

I would also like to thank the entire SEER research group for their help and support throughout this project. Additionally, I would like to acknowledge the LSU department of Petroleum Engineering for allowing these opportunities to happen. Thanks to Dr. Dongmei Coa of the LSU Shared Instrument facility for her help and training used in this work. I am also grateful for James Heathman and Darko Kupresan of Shell for their guidance and input on my work. As well as the Haliburton Drilling Fluids lab and Core Labs for their support on how to use equipment.

Lastly, I would like to thank my friends and family that have been there to encourage and support me thought this entire process.

Table of Contents

ACKNOWLEDGEMENTS ii

LIST OF TABLES v

LIST OF FIGURES vii

ACRONYMS x

ABSTRACT xi

CHAPTER 1: INTRODUCTION 1
1.1 Background 1
1.2 Objective 2
1.3 Methodology 3

CHAPTER 2: LITERATURE REVIEW 4
2.1 Wellbore Cementing 4
2.2 Lightweight Wellbore Cements 6
2.3 Application of Silica-Based Microspheres in Wellbore Cementing 10
2.4 Alkali-Silica Reactivity (ASR) 11
2.5 ASR Remediation Techniques 12
2.6 Wellbore Integrity 14

CHAPTER 3: EXPERIMENTAL METHODOLOGY 16
3.1 Microsphere Study 16
3.2 Cement Core Studies 17
3.3 ASR Expansion Study 19
3.3 Drying Samples 21
3.4 Helium Gas Porosimetry 21
3.5 Pressure-Pulse Decay Permeameter 21
3.6 Micro-Indentation Tests 22
3.7 Microstructure Analysis 25

CHAPTER 4: RESULTS 26
4.1 Microsphere Study 26
4.2 Cement Slurry at Ambient Conditions Tests 29
4.3.1 Porosity Analysis 32

4.3.2 Permeability Analysis 33
4.3.3 Indentation Mechanical Properties Analysis 34
4.3.4 Microstructure Analysis 36
4.4 Additional Microscopy Data 40
4.5 Expansion Study Results 42

CHAPTER 5: DISCUSSION 44
5.1 Mechanical and Petrophysical Property Analysis 44
5.2 ASR Expansion Analysis 49
5.3 Wellbore Integrity Time Line 52

CHAPTER 6: CONCLUSIONS AND RECOMMENDATIONS 54
6.1 Conclusions 54
6.2 Recommendations 54

REFERENCES 56

APPENDIX A: FULL HARDNESS AND YOUNG'S MODULUS DATA 60

APPENDIX B: FULL POROSITY AND PERMEABILITY DATA 71

APPENDIX C: MATERIALS USED IN EXPERIMENTS 72
B.1: Cement, Bentonite, Fly Ash, and Silica Flour 72
B.2: Microspheres 72
B.3 Metakaolin 72

APPENDIX C: ADDITIONAL SEM IMAGES 73

APPENDIX D: SAMPLE PREPARATION 78

APPENDIX E: LIST OF PUBLICATIONS AND PROCEEDINGS 80

VITA 81

LIST OF TABLES

Table 3.1: Mix proportions of cement by mass for sample preparation at 13 ppg then cured at ambient conditions 17

Table 3.2 Mix proportions of cement by mass for samples prepared at 13 ppg then cured at 70ºC (158ºF) 18

Table 3.3 Mix proportions of ASR expansion samples 20

Table 4.1. Young's Modulus and hardness values cured at ambient conditions 30

Table 4.2: Expansion test results change in water level. Values shown are the water level reading in the graduated cylinders, numbers shown are the average of three test 42

Table A.1: All Hardness and Young's Modulus values for dry samples with lithium nitrate cured at room temperature 60

Table A.2: All Hardness and Young's Modulus values for dry samples without lithium nitrate cured at room temperature 60

Table A.3: All Hardness and Young's Modulus values for wet samples without lithium nitrate cured at room temperature 61

Table A.4: All Hardness and Young's Modulus values for wet samples with lithium nitrate cured at room temperature 61

Table A.5: All Hardness and Young's Modulus values for samples containing only microspheres cured at 70°C 62

Table A.6: All Hardness and Young's Modulus values for samples containing microspheres and 2% lithium nitrate cured at 70°C 63

Table A.6: All Hardness and Young's Modulus values for samples containing microspheres and 5% lithium nitrate cured at 70°C 64

Table A.6: All Hardness and Young's Modulus values for samples containing microspheres and 8% metakaolin cured at 70°C 65

Table A.6: All Hardness and Young's Modulus values for samples containing microspheres and 25% metakaolin at 70°C 66

Table A.6: All Hardness and Young's Modulus values for samples containing microspheres and 15% Fly Ash cured at 70°C 67

Table A.6: All Hardness and Young's Modulus values for samples containing microspheres and 30% fly ash cured at 70°C 68

Table A.6: All Hardness and Young's Modulus values for samples containing microspheres and 15% silica flour cured at 70°C 69

Table A.6: All Hardness and Young's Modulus values for samples containing microspheres and 30% silica flour cured at 70°C 70

Table B.1: All sample data for porosity 71

Table B.2: All Sample data for permeability 71

LIST OF FIGURES

Figure 2.1: Showing the effects loss circulation has on the cement job as cement breaks into a weaker formation and flows into the formation instead of up the desired annulus. This leads to issues of improper zonal isolation, as well as strength issues of not having desired strength in desired areas 7

Figure 2.2: Reconstructed micro CT image of a foamed cement showing random size and distribution of gas bubbles in the cement (Pang et al. 2016) 9

Figure 3.2 ASR expansion test set up. Samples were crated with and without microspheres then cut to be flat then sealed in graduated cylinders shown in a high alkalinity solution. Levels of water and cement were recorded and motored as the cement was cured..... 20

Figure 3.3: Output from micro indentation test. The curve shows the depth of the indenter as a load is applied up until a maximum load where the sample is then unloaded. The unloading side of the curve is used to calculate hardness and Young's Modulus 23

Figure 4.1. Optical and SEM images on clean unreacted microspheres as well as EDS analysis of a microsphere 27

Figure 4.2. SEM images of microspheres after mixing and exposure to high alkalinity solution28

Figure 4.3. SEM images of the manufacturing flaws seen with the microspheres 29

Figure 4.4 SEM images of microspheres in the cement matrix curried at ambient temperatures 31

Figure 4.5: Graph showing the changes to average helium porosity values after one month of curing at 70ºC (158ºF) of dried samples. Showing that lithium nitrate and silica flour additive in the cement have little change on the dried porosity, and fly ash and metakaolin have large effects on the dried porosity of the samples. Error bars are showing standard divination of samples..... 33

Figure 4.6: Graph displaying the average permeability of three samples tested using pulse decay permeability after samples were cured for one month at 70ºC (158ºF). Trends show that all additive lower permeability except low percentages of lithium nitrate. Silica flour fly ash and metakaolin have the largest impact on decreasing the permeability. Error bars shown are standard deviations..... 34

Figure 4.7: Graphs showing changes in Young's Modulus and hardness taken from micro indentation testing. Values shown are averages of ten indentations on three different samples from each design after being cured for one moth at 70ºC (158ºF). All additives show an increase in hardness and Young's Modulus compared to neat. Trends show hardness increasing in all samples besides silica flour and lithium nitrate when compared to only microspheres. Young's modulus changes are not as large with lithium nitrate and silica flour increasing elasticity and metakaolin and fly ash not having large impacts expect low percentages of fly ash decreasing elasticity as compared to microspheres..... 35

Figure 4.8: optical images from cement samples containing only microspheres post curing showing cracks hinting at ASR formation 37

Figure 4.9: SEM images of microspheres in cement cured at 70ºC (158ºF) with different admixtures showing various reactions 39

Figure 4.10: Backscatter SEM images of microspheres in cement cured at 70ºC (158ºF) with metakaolin additives into the cement..... 40

Figure 4.11 Shows EDS spectrums of how the chemical composition changes around the microsphere from the center of the microsphere out the wall of the microsphere and then in the C-S-H of the cement matrix for samples containing 30% metakaolin and microspheres in cement cured at 70ºC (158ºF)..... 41

Figure 4.12: Graphic of how the sealed graduated cylinders changed from the samples with microspheres, with the water levels and cement level starting on distinguishable lines. After two weeks, the water had clearly been absorbed into the cement and the cement had risen above the line it started on..... 43

Figure 5.1: Percent change of Hardness, Permeability, and Young's Modulus values compared to neat cement samples of the same density. Shows a uniform increase in Young's Modulus a hardness because cement has a lower water percentage with microsphere addition and an almost uniform decrease in permeability because of lower water rate and more C-S-H growth..... 44

Figure 5.2: Comparison of Hardness. Young's Modulus, and permeability of samples showing percent change compared to only microspheres to see effects of different additives. Showing how metakaolin and fly ash increase Young's modulus and hardness while all other additives decrees this. While almost all additives decrees permeability..... 45

Figure 5.3: Two SEM images from two different studies on microspheres, this one and one by Halliburton. Both images show similar break down reactions of the microspheres and leaving only ASR..... 49

Figure 5.4: Shows how on the left as the cement shirks a microcannulas is formed around the cement allowing for fluids to flow up the wellbore, but by preventing this shrinkage as seen on the right flow up the wellbore is cut off because there is no microcannulas. 51

Figure 5.5: Well integrity life line showing show how the design portion of a well must address all other portions of the well life..... 53

Figure C.1: Additional SEM images of microspheres from solution 73

Figure C.2: Additional SEM images of microspheres in cement with no additives..... 74

Figure C.3: Additional SEM images of microspheres in cement with lithium nitrate 75

Figure C.4: Additional SEM images of microspheres in cement with metakaolin 76

Figure C.5: Additional SEM images of microspheres in cement with metakaolin 77

Figure C.1: Sample and experimental preparation 79

ACRONYMS

Ca	-	Calcium
Si	-	Silica
Li	-	Lithium
LiNo3	-	Lithium Nitrate
OH-	-	Hydroxyl
C-S-H	-	Calcium Silica Hydrate
SEM	-	Scanning Electron Microscopy
EDS	-	Electron Dispersive Spectroscopy
PPG	-	Pounds Per Gallon
ASR	-	Alkali-Silica Reaction
AAR	-	Alkali-Activated Reaction
ACR	-	Alkali-Carbonate Reaction
SCM	-	Secondary Cementous Material
P&A	-	Plug and Abandonment
API	-	American Petroleum Institute
W/C	-	Water Cement Ratio
DI	-	Deionized
RPM	-	Revolutions Per Minute
D	-	Darcy
MK	-	Metakaolin
SF	-	Silica Flour
FA	-	Fly Ash

ABSTRACT

Drilling through low pressure formations, either offshore or through depleted formations, requires the use of low density fluids to prevent lost circulation ensuring proper placement of cement for proper zonal isolation and structural integrity. Achieving these densities in cements can be done through foaming the cement, increasing water content, or using silica-based microspheres. Water extended cements are useful at densities down to 13 ppg below which only foaming and silica-based microspheres can be used. Each of these methods coming with individual limitations, with foamed cements being sensitive to high pressures and silica-based microspheres having chemical instability in the high alkalinity environment of wellbore cements.

This chemical instability creates a hydrophilic gel that is expansive and creates fractures in the cement as it expands, which is formally referred to as alkali-silica reactivity (ASR). Prevention of ASR involves the application of additives to the cement that act as a sink for the alkalinity and prevent the expansion of ASR. The sink works by having highly reactive silica in the cement slurry that reacts with the alkalinity during hydration so there is not enough alkalinity in the cement pore fluid to create ASR later in the life of the cement. Lithium nitrate also works as a prevention method by reacting with the silica before the alkalinity, thus creating a new layer of around the silica and preventing reactions with alkalinity.

This study looks at the effects of a high alkalinity cement environment onto the microspheres surface by visualizing the ASR occurring using Scanning Electron Microscopy (SEM). Then cement samples were created to compare the effects of lithium nitrate, fly ash, silica flour, and metakaolin have on cements created with silica-based microspheres. The microstructures of these samples were also imaged using SEM, visualizing that lithium nitrate, fly ash, and metakaolin having the largest impact on preventing reactions with the microspheres. The

mechanical properties of these changes were also tested using micro-indentation to give micro-hardness and Young's modulus. Petrophysical properties of the samples were tested for porosity and permeability. These values provide insight on how each additive's is effecting the long-term integrity of the cement.

CHAPTER 1: INTRODUCTION

1.1 Background

The possibility of lost circulation issues influence drilling operations around the world as drilling moves through deeper and depleted formations that were previously unreachable. In these drilling situations, extra precaution must be taken with all drilling fluids used downhole to minimize costly losses. In some cases, the drilling fluids lost can be more expensive than the oil that will be produced out of that formation. Additional cost will also be accumulated with non-productive times encountered to fix these issues. The repercussions associated with lost circulation while cementing can result in improper cement placement, allowing for the onset of wellbore stability issues, as well as undesirable fluid migration that can result in the requirement for remedial cement jobs. To prevent these issues, light-weight cements must be used.

Light-weight cements can be created through a variety of different methods, depending on the formation requirements. These methods work by mixing a low-density material into the cement to lower the bulk density of the cement, such as water extending, foaming, and/or adding silica-based microspheres. Each of these methods each come with their own drawbacks limiting their application. Increasing water content can only be done to 13 ppg (pounds per gallon) because below this point the water concentration becomes too high and the cement is unstable. Foaming the cement involves mixing nitrogen gas into the cement, ideally forming an even distribution of nitrogen bubbles throughout the cement matrix. Although, at high pressures this doesn't always happen, as bubbles are not evenly distributed and have random arrangements. Silica-based microspheres are small hollow beads that have extremely low densities that can be mixed into the cement and lower the density, but can react with the cement pore fluid causing the microspheres

to become unstable. Because of these drawbacks each method must have additional consideration before use.

In the case of silica-based microspheres, chemical instability issues associated with high silica content in cements leads to the onset of alkali-silica reaction (ASR). ASR forms as an expansive gel that absorbs the pore fluid. This expansion can lead to fracturing in the cement creating structural instability as well as channels for fluid migration. Prevention of ASR can be completed through a variety of methods, typically involving lowering the alkalinity of the cement pore fluid by mixing materials with high silica content into the cement. These compounds react with the cement and work as Secondary Cementous Materials (SCM) that provide strength to the cement and prevent ASR reactions. Additionally, lithium compounds have shown the ability to both lower the alkalinity of the pore fluid and prevent reactions with silica compounds.

1.2 Objective

The first objective of this study was to investigate the chemical stability of silica-based microspheres in a cement pore fluid as well as to understand the effects of ASR reactions on wellbore cements containing silica-based microspheres. The second objective was to investigate different ASR prevention methods that are used in civil engineering applications of concretes, for roads and building, and apply this knowledge towards ASR prevention in light weight wellbore cements containing microspheres.

1.3 Methodology

This study utilized a multi-tier approach to understanding ASR reactions with silica-based microspheres in wellbore cements and how to prevent these reactions. The first part of this study was a simple laboratory study to see the effects that high temperature and alkalinity have on microspheres. The next part of the study was investigating how the microspheres behaved in cement at ambient conditions as well as the effects that lithium nitrate had on these cements. Experiments were all conducted at near reservoir temperature comparing the effects multiple different ASR prevention techniques had on these cements. Additionally, this study added investigating how much expansion is associated with ASR at near reservoir temperature. These tests were completed on a laboratory scale with small cores that were kept at the same density for comparison purposes. After these tests, Helium Gas Porosimetry and Pulse Decay Permeability measurements were conducted to evaluate petro-physical changes the different additives had on the cement. Micro indentation was also conducted to investigate the changes in mechanical properties. Finally, scanning electron microcopy (SEM) and optical images were taken to observe changes in the microstructure of the cements.

CHAPTER 2: LITERATURE REVIEW

2.1 Wellbore Cementing

Wellbore cementing is a critical part of oilfield drilling and completions operations. It is an integral part in multiple stages of the wells development where each stage requires its own unique cement slurry design. Cementing is completed by pumping cement down through the casing shoe and then back up through the annulus between the casing and formation. Cement plays a role in well integrity by creating a hydraulic barrier between the casing and the formation as well as protecting and supporting the casing. During latter stages in a well's life, cementing can also be implemented to plug specific zones or the entire well by the way of plugging and abandonment (P&A) procedures (Nelson and Guillot 2006).

Almost all cements used in the oilfield are Portland cements. The cement is manufactured by heating mixtures of geo-materials, primarily limestone and clays, that contain high concentrations of calcium, silicon, aluminum, and iron. These materials are ground and heated in a kiln to temperatures between 2600-2800ºF (1400-1500ºC) (Konsmartka and Panarsee 1988). The mixture is cooled into spherical granules called clinker, which is ground with gypsum into a cement powder.

Table 2.1 Cement chemistry notion based on oxides as well as minerals (Taylor 1997)

Oxide	Notation	Mineral	Notation
CaO	C	Alite	C_3S
SiO_2	S	Belite	C_2S
Al_2O_3	A	Aluminate	C_3A
Fe_2O_3	F	Ferrite	C_4AF
H_2O	H		

Cement is composed of several oxide components which can be abbreviated for simplicity these oxides come together to form minerals which can also be abbreviated in Table 2.1.

When mixed with water, Portland cement begins a process known as hydration, which is a combination of dissolution and precipitation reactions. During hydration, the cement reacts with water to form three main components: calcium hydroxide, Calcium Silicate Hydrate ($3CaO{\cdot}2SiO2{\cdot}3H2O$, C-S-H), and aluminum trisulfate, also known as ettringite (Taylor 1997). C-S-H accounts for ~50% of the hydrated cement accounting for most of the strength of the cement. Calcium hydroxide and ettringite are both crystal structures formed in the cement paste. Calcium hydroxide accounts for ~15% of the cement paste, which forms uneven hexagonal crystals and is stable at high pH. Ettringite, along with other products of the C_3A and C_4AF reactions, accounts for 15-25% of the cement paste in the form of needle shaped crystals (Taylor 1997).

Hydrated cement paste is a rock-like material of low permeability with the porosity ranging from 2-20% of the volume, depending on the cement water (c/w) ratios and the degree of hydration (Jennings and Thomas 2009). This porous region is filed with fluids that have free, unreacted ions available for alkali attack on silica materials present in the cement slurry. The degree of hydration is the percentage of completion for all the reactions that have taken place and can range in amount of time it takes to reach full hydration. 28 days is normally accepted as an appropriate amount for hydration time to reach close to the cement's final overall strength (Mehta and Monteriro 2006).

During the hydration process, the porosity and permeability decrease as the strength increases due to the various reactions taking place, which is referred to as a process known as hardening (Mehta and Monteriro 2006). Hardening occurs because of the growth of C-S-H and can take varying amounts of time to reach completion depending on temperature conditions. As hydration has undergone, precipitation of different products changes over time with ettringite

controlling most of the early time reactions, while C-S-H and calcium hydroxide control the later reactions. These reactions are what cause the decrease in porosity and permeability as well as the strength development. Because of the increased temperatures in wellbores, the rate of hydration increases in cement, which causes these reactions rates to increase (Zhang et al. 2010).

The American Petroleum Institute (API) classifies nine different Portland cement types, denoted alphabetically. These different types of cements are distinguished by different compositions and partial sizes, allowing them to be used in different conditions. (API 2013). Cement additives become necessary to meet the requirements of different formation properties and drilling requirements. Additives are split into six different categories: density control, setting time control, lost circulation control, filtration control, viscosity control, and special additives for unique circumstances (Nelson and Guillot 2006).

2.2 Lightweight Wellbore Cements

During drilling operations, there is a constant need to monitor the density of the drilling fluid to keep the density in what is known as the drilling window. This drilling window is the difference between the formation pore pressure, the pressure of the fluid within the pores of the rock, and the fracture pressure, which is the maximum stress the formation can handle before it breaks (Lavrov 2016). This concept is important because if the fluid pressure inside the drill column falls below the pore pressure, the fluids inside the rock will begin to flow into the well while drilling, which is known as a kick. Alternatively, if the pressure inside the drill column becomes greater than the fracture pressure, the drilling fluid will break the rock and flow into the formation rather than back up the drill column. This is known as lost circulation (Lavrov 2016). A diagram of loss circulation and its effects can be seen in Figure 2.1.

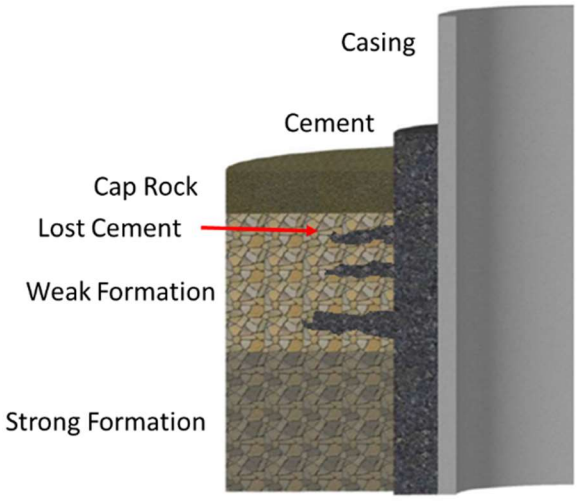

Figure 2.1: Showing the effects loss circulation has on the cement job as cement breaks into a weaker formation and flows into the formation instead of up the desired annulus. This leads to issues of improper zonal isolation, as well as strength issues of not having desired strength in desired areas

Cementing also must follow these same requirements. The density of the cement must be controlled to assure the cement stays inside of the drilling window. This can be difficult in low pressure formations, especially those encountered at shallower depths offshore or when drilling through depleted formations. In these cases, it becomes necessary to decrease the density of the cement through a variety of different methods. Failure to achieve this results in lost circulation of the cement because the cement flows into the rock formation and not into desired annular space, causing very costly remedial treatments (Lavrov 2016). At the same time, these low-density cements still must maintain wellbore stability and zonal isolation as is expected for any cement (Schultz 2001).

The easiest way to achieve a lower density wellbore cement is by utilizing water extension. This process is completed by increasing the w/c (water to cement) ratio from the standard .38 w/c to a higher water content with .87 w/c ratio being around the higher expectable limit. Additionally,

this higher w/c ratio reduces the compressive strength of the cement as well as increases the cement's porosity and permeability (Mehta and Monteiro 2006). Because of these limitations, water extension is typically not used at densities below 13 ppg (1.55 g/cm3).

To achieve cement densities below the 13 ppg (1.55 g/cm3), the industry employs two methods: foaming cement and the addition of hollow silica microspheres. Both methods can be used to reach similar densities, but each come with their own limitations. Foam has a sensitivity to pressure, and silica microspheres have a sensitivity to pH. However, since both methods can be used to achieve densities, the deciding factor for selecting the optimal method in each field scenario depends on the durability of cement under those conditions. For example, drilling in low pH formation waters would be more suitable for foamed cements, as they have sufficient alkali content to provide protection of casing against corrosion.

Foaming cement is achieved by mixing nitrogen in with cement while pumping the cement into the well. This causes small bubbles of nitrogen gas to become entrapped in the cement mixture, effectively lowering the density of the cement by having a predetermined volume percentage of the cement become entrapped gas (Pang et al 2016). A reconstructed micro CT image of a foamed cement can be seen in Figure 2.2 where all of the gas bubbles can be seen distributed in the cement. When done correctly, this method can accurately possess the required density as well as desired structural strength. Foamed cements that are considered stable will have an even distribution of small nitrogen gas bubbles throughout the cement. The issue with foamed cements is that they are hard to simulate in the lab to accurately represent what happens in the field (Pang et al. 2016) (Gieger et al 2016) (Kutchko et al 2015) (Kutchko 2016). This is because of differences in pressures in the lab and in the field, as well as differences in preparation of foamed cements samples in the lab and in the field, making it hard to conclude that the cement will be

stable in the field based solely off lab results. In some cases, lab results show that the slurry has the potential to be unstable, but are still used in the field. One famous example of this was the Deepwater Horizon blowout, where lab test for the foamed cement said the cement would be unstable and was still used and resulted in cementing failure (Chief counsel report).

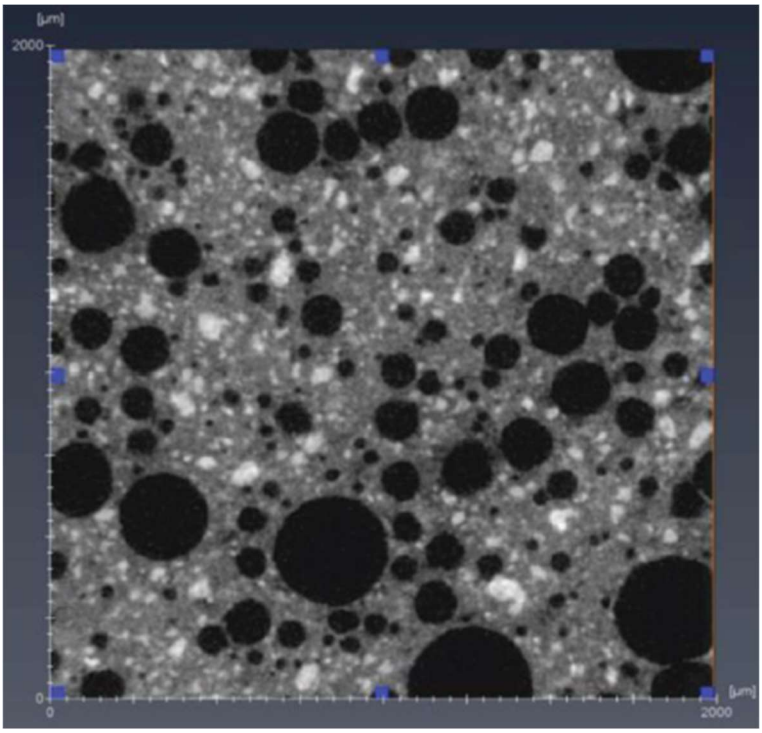

Figure 2.2: Reconstructed micro CT image of a foamed cement showing random size and distribution of gas bubbles in the cement (Pang et al. 2016)

If foamed cement is unstable, the nitrogen gas will not stay trapped in small separate gas bubbles in the cement, but instead the gas bubbles will travel up through the cement as it sets, creating large channels of nitrogen gas inside the cement column. This is a problem because it creates a structurally weak point in the cement, as well as creating a large path for formation fluids to move through the cement.

2.3 Application of Silica-Based Microspheres in Wellbore Cementing

Silica microspheres are the alternative to foaming cements. They are capable of withstanding pressure increase and maintaining mechanical stability at subsurface conditions. The microspheres are hollow silica spheres composed of borosilicate silica. They range in size and specific gravity depending on product line and manufacturer. Most of the microspheres are 30 microns in diameter and have a specific gravity around 0.5. The different product lines represent the microspheres' individual composition and pressure ratings—higher density microspheres can withstand higher pressures. The microspheres can be mixed in with the cement during the mixing processes to be evenly distributed throughout the cement. These microspheres have been field tested and proved to provide the necessary characteristics for pumping a job in difficult formations both onshore (Carver et al. 2011) and offshore (Abdullah 2013).

Extensive research has been conducted on microspheres in laboratory settings investigating the mechanical properties of the microspheres, and the cements they are used in. These studies showed that the microspheres can withstand manufactured supplied applied pressures (Sabin 2005). Additionally, higher pressure rated microspheres have minimal fracturing during mixing only slightly changing cement density after mixing (Sabin 2005). With this basic test completed, mechanical properties of lightweight cements achieved through water extension, foaming, and microspheres were compared. The cements that contain microspheres showed higher tensile strengths, young's modulus, and effective compressive strength then those cements that were foamed (Sabin 2005). The microspheres cements also had the lowest water permeability and air permeability (Sabin 2005). The final part of the study showed the downfall of the microspheres as the cements were tested for expansion and compressive strength over a year long time frame.

The results also showed that the samples were expanding and losing compressive strength (Sabin 2005), showing the potential for the existence of alkali-silica reactivity (ASR).

2.4 Alkali-Silica Reactivity (ASR)

Hydrated cement contains significant amounts of small pores in its structure. These pores contain a pore fluid that is highly alkaline (pH > 12.5) due to high percentages of hydroxyl (OH^-). In addition to the OH- in the fluid, there are also large percentages of Ca^{2+}, K^+, and Na^+ (Swamy 1992). In the presence of alkali active additives in the cement, hydroxyl will react with these addatives causing expansion and fracturing of the cement. This phenomenon is known as alkali-aggregate reactions (AAR) and is split up into two main categories: alkali-carbonate reaction (ACR) and alkali-silica reaction (ASR) (Dhir et al. 2009). ACR occurs when dolomite is present in the cement structure and is attacked by the pore fluid, breaking apart the dolomite and making cracks to allow the reactions to continue creating more reaction products and causing expansion (Fournier et al. 2000).

ASR occurs when imperfect crystalline silica (SiO_2) is present in the cement matrix and is attacked by the hydroxyl in the pore space of the cement through a series of reactions. The first reaction occurs when the silicon and oxygen bonds are attacked by hydroxyl molecules in the pore fluid, and then are replaced by OH forming silanol bonds (Swamy 1992).

$$SiO_2 + OH^- \rightarrow SiOH$$

Next, these bonds are further broken down by the hydroxyl breaking apart the silicate into an anion.

$$SiOH + OH^- \rightarrow SiO^- + H_2O$$

This silicate anion is then prone to react with the free cations in the pore fluid. If there is a high concentration of calcium cations in the system, the reaction will form a C-S-H gel, which can be beneficial, but if there is not a high enough concentration of calcium cations to control the gel reactions, the gel becomes a concerning high-alkali gel. This gel is hydrophilic and will absorb the water around it and begin to swell. This phenomenon is known as ASR. The swelling becomes especially problematic because it can cause the cement structure to crack as the gel expands, lowering the cements structural strength. In cements that contain glass additions, such as silica microspheres, this phenomenon becomes especially concerning because the additional silica acts as a base for the gel to grow on, causing significant expansion (Dhir et al. 2009).

Though the ideas of ASR formation are understood the factors leading up to ASR formation and the actual ASR structure is often very different. The properties of the silica used to form ASR as well as the size of the silica grains can have large impacts on the formation of ASR with smaller grain sizes expanding faster (Diamond and Thaulow 1974). Then temperature has large effects on the reaction rate for ASR, but not on the structure of ASR like C-S-H (Fournier et al. 1991). Pressure also has an influence on the creation of ASR (Broekmans 2004) but not as significant as temperature. Once ASR has formed the the structure of the gel is not always the same but have varying levels of silica calcium and other alkalis (Knudsen and Thaulow 1975) (Regourd and Hornain 1986). Once ASR has begun production it will continue to grow and change forms as the gel absorbs more water and cations in the solution changing the structure of the ASR matrix further (Kawamura et al. 1996).

2.5 ASR Remediation Techniques

Due to the widespread occurrence of ASR, extensive research has been conducted in trying to prevent the expansion caused by ASR in cements. This research has led to two main ideas on

how to prevent or control ASR in cements. The first method to accomplish this is done by adding silica grains, fly ash, or slag. These additions act like a sink for the hydroxyl and lower the pH of the pore fluid, preventing the SiO_2 from reacting (Tang et al. 2015). Though this method works well for preventing the ASR reaction, it often requires high mixture percentages of additives to prevent the reaction and lowering pH prevents corrosion defense of metal components in a structure (Duchesne 2001). Metakaolin is an effective compound that works as a pozzolanic material for preventing ASR and leading to higher strength development and lower pore space in the cement (Shen et al. 2017) (Moser et al. 2010). These prevention mechanisms are what is known as pozzolanic materials or supplementary cementitious materials (SCMs). These materials have high silica content and work by reacting with the initial reactants in the cement to form C-S-H and binding up hydroxyl in the solution to prevent ASR later in the life of the cement.

The second method being investigated for ASR prevention is the use of lithium based compounds. Lithium based compounds used to prevent ASR are also theorized to provide a range of beneficial mechanisms (Tremblay et al. 2010). Like other prevention methods, these compounds will decrease the pH of the pore fluids, and/or cause other changes to the chemistry of the pore fluid. Additionally, it is theorized that an early formation of Si-Li reaction products will act as a physical barrier to prevent further reactions. This SI-Li reaction product is either crystalline or amorphous, and is very little or completely non-expansive. Also, lithium compounds have being tested to show that this creates a higher solubility of the silica preventing the formation of ASR gel (Tremblay et al. 2010).

The most effective lithium compound at preventing ASR is lithium nitrate ($LiNO_3$). This compound has been shown to prevent the effects of ASR by acting like excess calcium in the pore fluid, and reacts creating a C-S-H type structure (Leeman et al. 2014. Because of this effect, many

studies have shown this method as an effective ASR mitigation technique (Leeman et al. 2014) (Schneider et al. 2008). Figure 2.3 shows a diagram of how ASR forms as well as how lithium nitrate works to prevent ASR.

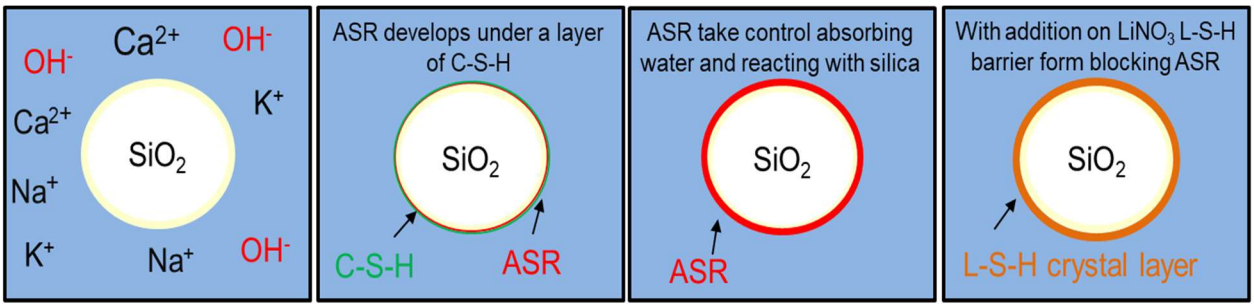

Figure 2.3: Diagram of how the high alkalinity solution in cement pores interacts with microspheres and breaks them down to form ASR. Then the image on the right shows how lithium nitrate works to prevent ASR

2.6 Wellbore Integrity

Wellbore integrity issues impact oil and gas operations around the world. These issues arise through some form of cement or casing failure that allows for gas flow through the annulus which would otherwise be impermeable. One way these pathways can form is through debonding between cement and rock or casing/ tubing barrier. This debonding occurs because of improper mud cleaning as the cement was pumped into place resulting in improper cement bond, or because of shrinkage as the cement sets. Either of these methods allow for a micro annulus to form on the outside of the cement column were gas can flow. Additionally, flow can occur in the cement due to fractures in the cement that are formed as the casings are exposed to thermal or pressure changes throughout the life cycle of the well applying stresses to the cement. Furthermore, if there is sheer stress placed on the cement, fractures can form along the cement shear. Flow can also occur between connected pores in the cement shear, as seen in poorly foamed cements. Furthermore,

gas can flow through the annulus due to cracks in the casing or tubing caused by corrosion where there isn't cement on the back side of the steel to block flow (Davies et al. 2014).

Though these issues seem simple in their formation the effects are wide spread and very costly in the oil and gas industry. In the Marcellus formation between 2008 to 2013 of 6466 well producing, 3.4% showed to have annular gas flow (Vidic et al. 2013). In Norway 18% of 406 offshore wells tested shoed to have wellbore integrity issues (Vigines and Aadnoy 1010). In the United Kingdom in 2005, 10% of wells had to be shut in because of integrity issues (Burton 2005). In the United States, these numbers are even worse with 43% of 15,500 wells drilled in the Gulf of Mexico show integrity issues (Brufato et al. 2003). These numbers show the widespread occurrence of these problems that cost the industry large sums of capital, needing to work over wells to fix these issues or shutting in these wells early to try to prevent total failure. Failure to address these issues result in environmental issues as gas escapes the wells, as well as safety issues if the well completely fails.

CHAPTER 3: EXPERIMENTAL METHODOLOGY

To understand the reactions occurring with microspheres in the high alkalinity environment of the cement matrix, as well as the effects of these reaction and how to prevent ASR, a multiple stage experiment setup was developed. This involved looking at microspheres in a high alkalinity solution so see the reactions that occur with microspheres. Next the microspheres were mixed in with cement and allowed to cure at ambient temperatures, to see how the cement and microspheres would interact. Then cement was cured at temperature with different ASR preventative additives used to see the effects on ASR and the cement. All the cement samples were cured for 28 days, samples were tested for mechanical, petro-physical, and microstructure properties. Additionally, a study was completed to show the expansive properties of ASR and the negative effects this can have on the cement.

3.1 Microsphere Study

Knowing that microspheres in a cement matrix were leading to the onset ASR, an initial study was conducted simplifying the cement pore fluid to react with the microspheres. To accomplish this, a high alkalinity solution was created to represent cement pore fluid. This solution was created by mixing sodium hydroxide with deionized water until a pH of approximately 13 was reached. Also, a separate solution of deionized water was used as a control. Separate mixtures were created with the different microsphere samples and the two solutions. One gram of microspheres was mixed in with 20 mL both solutions. After which the mixtures were placed into a temperature chamber set at 80ºC (176ºF) for one week. After this time, the samples were removed from the chamber, dried, and prepared for imaging.

The effects of different mixing rates were also investigated. This was done to see how the microspheres would hold up in a field mixing process, as well as to assess how microspheres can be mixed for cement samples. Five grams of microspheres were mixed with 100 mL of deionized water. These were mixed in a Waring laboratory blender at approximately 14,000 revolutions per minute (RPM) and 3,000 RPM separately for 30 seconds. A third process was also conducted, shaking the mixtures around by hand for 30 second to simulate light mixing. After, all the samples were dried for imaging.

3.2 Cement Core Studies

Cement studies were completed in two parts the first being at ambient conditions and only testing lithium nitrate for prevention and the other being at reservoir temperature and testing multiple prevention mechanisms. All cement slurries were designed at 13 ppg (1.55 g/cc) for consistency when testing, as well as all samples used the same percentage of microspheres to allow for the same amount for reaction surface area. The mix proportions used in the ambient condition test can be seen in Table 3.1. All cement used is Haliburton Class H cement. This initial test was used to see how the cement would react with the microspheres as well as gain an understanding of how prevention works and what influence lithium nitrate would have on the cement.

Table 3.1: Mix proportions of cement by mass for sample preparation at 13 ppg then cured at ambient conditions

Design	Only Microspheres	Microspheres and $Li(NO)_3$
Cement	1	1
Water	.58	.62
Bentonite	.02	.02
Microspheres	.08	.08
$Li(NO)_3$	0	.05

The second set of cement slurries were designed at reservoir temperatures to test a variety of different ASR prevention mechanisms. These samples were designed according to the mix proportions shown in Table 3.2. Mix percentages were chosen to all within ASR prevention mechanisms set forth by the U.S. Department of transportation for highways (U.S. Department of transportation 2012).

Table 3.2 Mix proportions of cement by mass for samples prepared at 13 ppg then cured at 70ºC (158ºF)

Design	Neat	Only Microspheres	2% $LiNO_3$	5% $LiNO_3$	8% MK	25% MK	15% SF	30% SF	15% FA	30% FA
Cement	1	1	1	1	1	1	1	1	1	1
Water	.87	.58	.59	.61	.63	.75	.66	.75	.68	.8
Bentonite	.02	.02	.02	.02	.02	.02	.02	.02	.02	.02
Microspheres	-	.08	.08	.08	.08	.08	.08	.08	.08	.08
$Li(NO)_3$	-	-	.02	.05	-	-	-	-	-	-
Metakaolin	-	-	-	-	.08	.25	-	-	-	-
Silica Flour	-	-	-	-	-	-	.15	.3	-	-
Fly Ash	-	-	-	-	-	-	-	-	.15	.3

Both sets of samples were created following the same procedure. Samples were created in a Waring laboratory blender per API recommended practices (API 10B-2 2015). Mixing was completed in a 4 litter, 3.75 horsepower Waring laboratory blender. The bentonite was prehydrated (i.e. blended with water) at approximately 16,000 RPM for five minutes. After this time, all other solids besides the microspheres were mixed in at approximately 20,000 RPM for 35 seconds. Microspheres were mixed in by hand after this time with a spatula until even distribution of microspheres was noted visually. Microsphere mixing by hand is not necessary because mixing only damages a small portion for the microspheres but this was suggested by the manufacture as well as in the lab appeared to be better at more evenly distrusting the microspheres.

Samples were then poured in 3x1 inch (7.63x2.54 cm) cylindrical brass molds. Samples were kept in these molds at atmospheric conditions for 24 hours. After, they were removed from the molds and placed in a sealed solution of deionized water and calcium hydroxide at a pH of around 13. These containers were placed in an environmental chamber kept at 70ºC (158ºF) and 100% relative humidity to hydrate, or left sealed on the benchtop depending of which mix study was being completed. After 28 days, the samples were prepared for testing.

All cores tested were cut to 2 in (5 cm) in length by cutting portions of the cores off both ends. This was done to remove any defects that would be on the ends of the cores and ensure flat surfaces on the end of the cores.

3.3 ASR Expansion Study

An additional method of seeing the effects of ASR as well as to ensure that ASR was happening an Expansion test was also conducted. To do this two-different cement slurries were created. One slurry with microspheres and another without, these slurries mix proportions can be seen in Table 3.3. The slurry without microspheres was created at 13 ppg (1.55 g/cc) and the slurry with microspheres was created at 9 ppg (1.07 g/cc), this was done to test a high percentage of microspheres mixed in the slurry to ensure maximum reaction in a short period of time. All samples were created in the previously noted methods. After being removed from the brass molds samples were cut to 2 in (5 cm) so they were smooth on both ends. They were then placed in 100 cc Pyrex graduated cylinders. The graduated cylinders were then filed with the same 13 pH calcium hydroxide and DI water solution used before to the 50-cc line. The location in the graduated cylinder of the cement and the water were recorded then the cylinders were sealed at the top with a cork stopper. The samples were then placed in the environmental chamber at 70ºC (158ºF) and 100% relative humidity. Samples were kept in the environmental chamber for 3 months and

observations were made of the water level as well as the cement top level periodically throughout this time. Figure 3.2 shows the samples inside the graduated cylinders before being placed into the environmental chamber. Three samples of both mixes were used tested.

Table 3.3 Mix proportions of ASR expansion samples

Design	No Microspheres	Microspheres
Cement	1	1
Water	.87	.9
Bentonite	.02	.02
Microspheres	-	.45

Figure 3.2 ASR expansion test set up. Samples were crated with and without microspheres then cut to be flat then sealed in graduated cylinders shown in a high alkalinity solution. Levels of water and cement were recorded and motored as the cement was cured.

3.3 Drying Samples

All samples that were imaged as well as samples that were tested for porosity had to first be dried. Drying samples required that all samples were soaked in acetone of 24 hours. This would allow most of the cement pore fluids to be replaced with acetone that way minimal precipitants were formed during the actual drying out process. After this time samples were moved to an oven and kept at 70ºC (158ºF) for 24 hours to remove all fluid from samples.

3.4 Helium Gas Porosimetry

Porosities were determined for three cores from each of the different mix designs. This was completed using an Ultragrain GrainVolume Porosimeter, UGV-200 from Core Labs. This devise measures the pore volume of the dried samples. Bulk volume is pre-calculated for the sample, then a 10-cc camber is filled with helium gas and the core is sealed in another container of known volume. The pressure is recorded in the 10-cc chamber then the two chambers are opened to one another and the pressure is recorded again. Using this pressure change a new volume is calculated for the pore volume of the sample. Then by dividing the pore volume from the bulk volume of the sample a porosity is calculated.

3.5 Pressure-Pulse Decay Permeameter

Permeability measurements can be completed through a variety of different flow through experiments, for this study Pressure- Pulse Decay (PDPL) was completed using a Core Labs PDPL model CFS-200. This method was chosen because unlike steady state permeability measurements

that can take long periods of time and permeability change as cement hydrates during these experiments can be run in much shorter time frames (Schere et al. 2006).

In this method cores were loaded into a rubber sleeve inside of a pressure vessel. The vessel was then filled with water and raised to a confining pressure of 5000 psi (34.4 MPa). Then water was flown through the core by setting the pressure on one side of the core to 400 psi (2.76 MPa) and the other end was raised 500 psi (3.45 MPa). After, water flows across the core causing a pressure differential that is recorded. The natural log of this pressure differential is plotted against time and the slop of that line is then calculated. With this slope, a permeability is calculated using the equations below.

$$k = \frac{\phi \mu m C_f}{a^2}$$

$$atana = \frac{V_P}{V_1}$$

Where K= permeability, ϕ= porosity, μ= water viscosity, m= slope, C_f = water compressibility, V_P= Core pore pressure, V_1= core bulk volume

3.6 Micro-Indentation Tests

A Nanovea Micro/Marco Module was used to test the micro mechanical properties of the samples. This device works by running an independence force and displacement sensor as the micro indenter penetrates the sample to micron depths as an optical sensor measures displacement. The tip that is used to penetrate the sample is of a known geometry. This tip applies a constant preset normal load onto the sample until a load limit is reached, then this load is held constant for

a period of time followed by an unloading process occurring. During this loading and unloading process both the loads and displacement are plotted and from this plot mechanical properties can be calculated. For this study hardness and Young's Modulus were used.

In this study, all samples were tested using a Vickers diamond tip with a poisons ratio of .3. A maximum load of 10 N (2.25 lbf) was applied with a loading and unloading rate of 15 N/min (3.37 lbf/min) with a 30 second wait time between the loading and unloading process. An example loading and unloading curve can be seen in Figure 3.3.

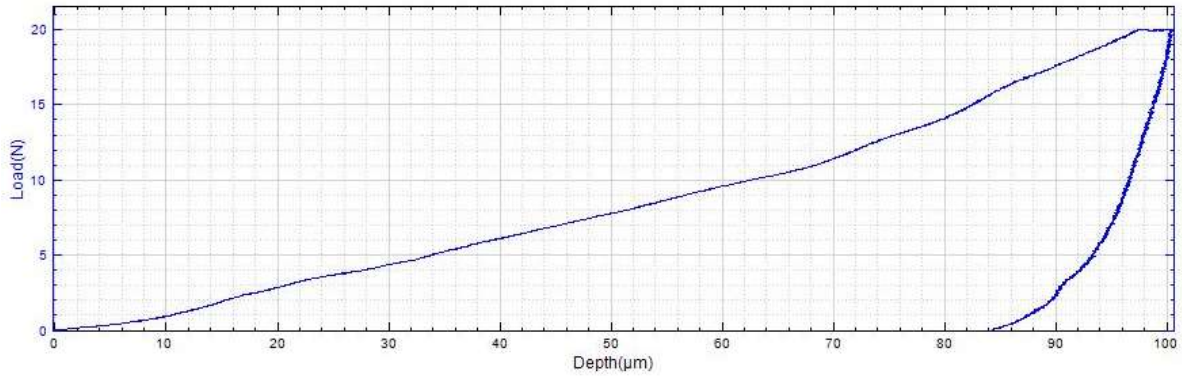

Figure 3.3: Output from micro indentation test. The curve shows the depth of the indenter as a load is applied up until a maximum load where the sample is then unloaded. The unloading side of the curve is used to calculate hardness and Young's Modulus

The information taken off the plot in Figure 3.3 is the used to calculate the Young's Modulus and hardness. Hardiness is the easiest to be calculated by dividing the maximum load (P_{max}) by the Contact area (A_C).

$$H = \frac{P_{max}}{A_C}$$

Where contact area is calculated by using the indenter area function for the specific geometry of the indenter. For Vickers inventors, the following equations are used

$$A_C = 24.5\, h_c^2$$

$$h_c = h_{max} - \epsilon \frac{P_{max}}{S}$$

Where ε is a constant for the geometry of the indenter, in this case .75, h_{max} is the maximum displacement of the indenter and S is stiffness calculated from the strait part of the unloading curve.

Young's Modulus is then calculated from the below formula

$$E = \frac{1}{(1 - v^2)(\frac{1}{E_r} + \frac{1 - v_i^2}{E_i})}$$

Where E_i and v_i are the Young's modulus and Poisson ratio of the inventor, v is the Poisson's ratio of the sample, and E_r is the reduces modulus calculated by

$$E_r = \frac{\sqrt{\pi}}{2} \frac{S}{\sqrt{A_c}}$$

All samples tested in this study were indented multiple times across the surface of the sample. These values were recoded and then averaged, to give a property for this sample. This was done because the structure of cement is very heterogeneous, and because the tip is so small it only gets a value of one crystal of the cement structure. So, by having multiple values from across the surface of the cement a more accurate value of the cement can be calculated.

Typically, in wellbore cementing compressive strength is tested for Young's Modulus values. The differences between these tests are that micro indention is nondestructive and typically have a smaller standard deviation. Values tested from compressive strength and through indentation have shown to have similar results for Young's Modulus (Nanovea 2016). Additionally, extensive research has been completed using this machine with heterogeneous materials like shale to show the ability to produce meaningful data (Du et al. 2017).

3.7 Microstructure Analysis

To visualize the microstructures of the cement samples a variety of different imaging was completed. All samples that were imaged, were dried according to the sample drying procedure presented earlier. Then samples were polished in stages down to a 10-micron surface with a sonic bath done between each stage to shake away all the previous polishing debris. For non-optical imaging, a conductive coating of carbon was applied to the samples to prevent charging.

For optical images, a Lecia DM2500-P modular polarization optical microscope was used to see the cement under medium magnification.

For high magnification scanning electron microcopy (SEM) and electron dispersive spectroscopy (EDS) was conducted. A dual beam-focused ion beam microscopy, FEI Quanta 3D FEG/SEM was used to do this imaging. Imaging was completed at 20 KV and 27 pA. These high magnification images generated through SEM give a high-resolution image of the microstructure of the cement interactions with the microspheres with the different additives. SEM works by sending a focused high energy electron beam at the surface of the sample. Interactions between the sample and the electrons create secondary electrons, backscatter electrons, and X-rays that are then detected and give a picture of the samples topography and composition (Goldstein et al. 2007).

CHAPTER 4: RESULTS

4.1 Microsphere Study

The initial microsphere study was conducted to visually see the interactions that a high alkalinity fluid has on the microspheres, as well as to see how the microspheres would hold up to mixing. SEM and optical images of microspheres directly from the manufacture are shown in Figure 4.1. These images show that microspheres have clean hard walls that have not been interacted with. These images are used to compare to the microspheres post reaction. Figure 4.1 also shows an EDS analysis of clean microspheres. This spectrum shows the presence of carbon because these samples were coated in a conductive carbon coating for SEM. The rest of the spectrum shows mostly Si, O, and B with small amounts of Na and Ca. The Si:O ratio is at about 1:2 showing the majority of the microsphere is SiO_2, then there is also a large amount of B which makes sense considering the microspheres are a soda-lime borosilicate glass.

To see the effects that mixing as well as exposure to temperature in a high alkalinity solution had on the microspheres only SEM was used. These images can be seen in Figure 4.2. These images show that the high alkalinity solution is clearly reacting with the microspheres, with images showing two stages of the reaction. The first stage of the reaction seen is reaction pits across the surface of the microspheres. Then in later stages of the reaction the full surface of the microsphere has been reacted leaving only a reaction product layer like the structure of C-S-H in place of the microsphere wall. Then with the microspheres that were mixed, only the microspheres that contacted the mixing blades have fractures in the wall indicative of high impact forces. The microspheres that were hit at high speeds had larger impact fractures. Samples mixed by had showed no difference from the clean new samples.

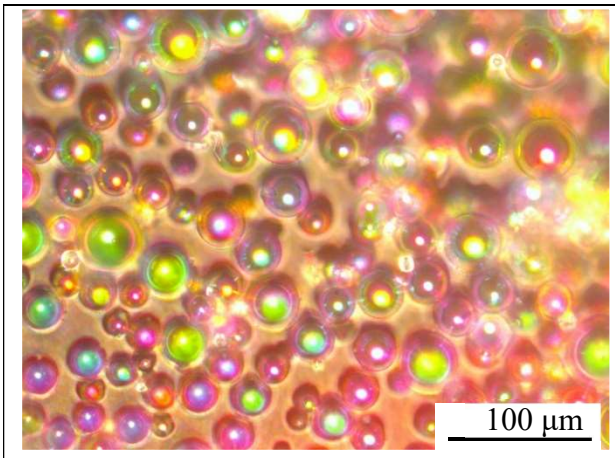

A. Optical image or clean unreacted microspheres straight from manufacture. Microspheres are intact with minimal flaws

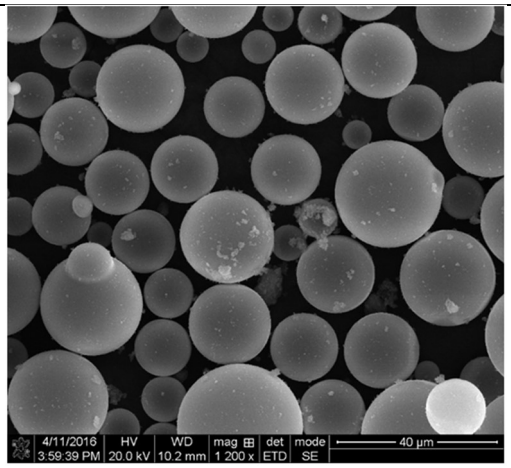

B. SEM image of clean unreacted microspheres. Some debris is on the outside of the microspheres, minimal flaws on the microspheres but no reactions

Element	Weight %	Atomic %
B	22.05	32.19
C	9.17	12.05
O	41.56	41.01
Na	3.2	2.2
Si	18.35	10.31
Ca	5.68	2.24

C. EDS spectrum of analysis of a microsphere, carbon present is from carbon coating on microsphere, majority Si and O representing SiO_2 with addition on boron because the microspheres are a soda-lime borosilicate glass

Figure 4.1. Optical and SEM images on clean unreacted microspheres as well as EDS analysis of a microsphere

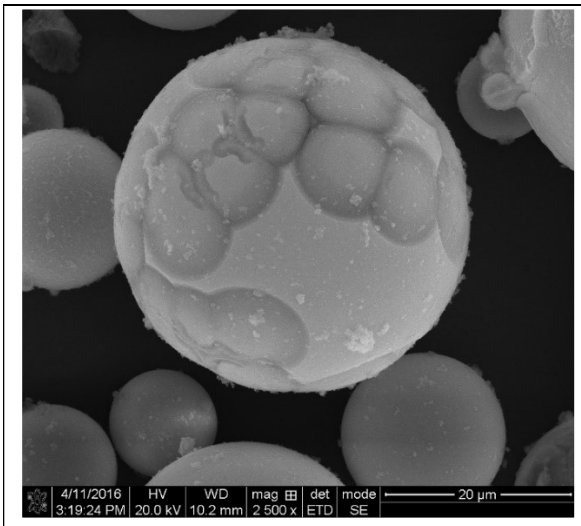	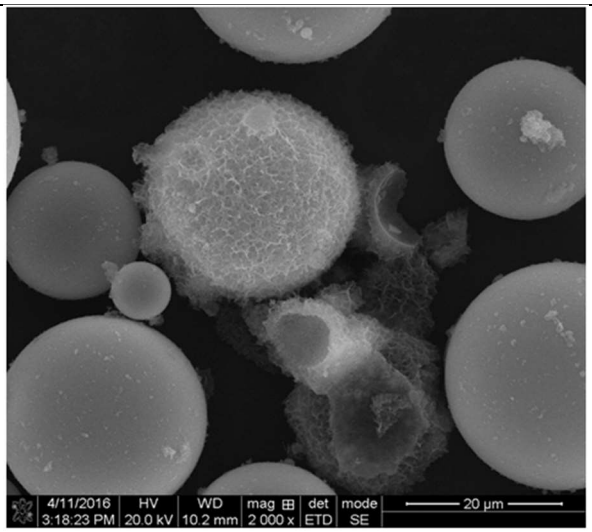
A. SEM image of microsphere after exposure to high alkalinity solution and temperature for one week. Showing initial stage of the reaction where the solution begins reacting with microspheres creation reaction pits on the surface of the microsphere	B. SEM image of microsphere after exposure to high alkalinity solution and temperature for one week. Showing later stages of the reaction where the solution has fully reacted with the microsphere leaving only a reaction product layer resembling C-S-H where the microsphere wall was
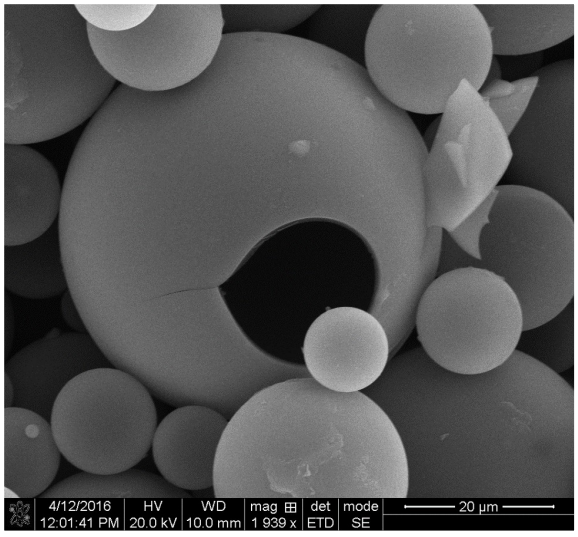	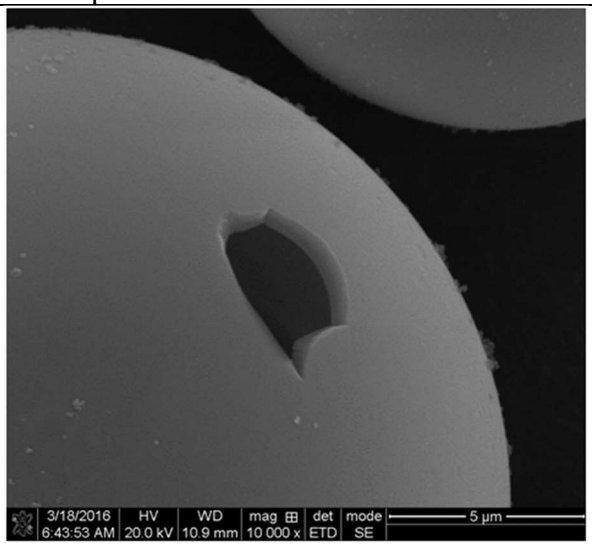
C. SEM image of a microsphere after being impacted with the mixing blade of the mixer at 14,000 RPM. Crack created in microsphere is a clean hole only caused by a high impact force.	D. SEM image of a microsphere after being impacted with the mixing blade of the mixer at 3,000 RPM. Crack created in microsphere is a clean hole only caused by a high impact force. Crack is not as big as the crack created by the higher RPM's

Figure 4.2. SEM images of microspheres after mixing and exposure to high alkalinity solution

Also, noted during this investigation of the microspheres was many manufactures defects. These defects appeared to be more reactive with the high alkalinity solution as well as would hinder the microspheres performance when trying to decrease bulk density of cement. SEM images of these defects can be seen in Figure 4.3, and can be split into two different categories. One of these effects is when the microspheres would form inside of other microspheres. The other defect was when larger masses of microspheres would form together around a solid central matrix.

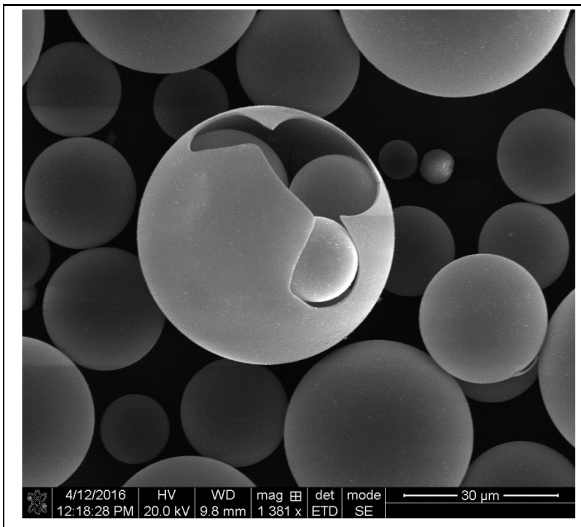

A. SEM image of one flaw in the manufacturing design of the microspheres where microspheres would form inside of other microspheres. This would lead to an increase of the bulk density of the microspheres.

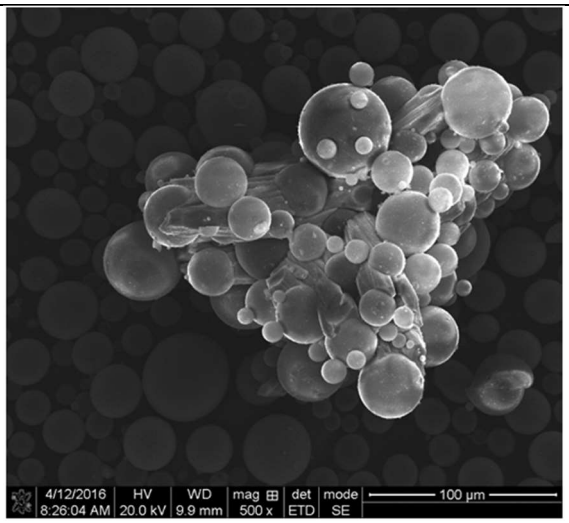

B. SEM image of flaw in manufacturing process of the microspheres where many microspheres would form together into one large mass around a solid central matrix. This would lead to an increase in the bulk density of the microspheres.

Figure 4.3. SEM images of the manufacturing flaws seen with the microspheres

4.2 Cement Slurry at Ambient Conditions Tests

Test of the microspheres in cement at ambient conditions were completed to begin to get an understanding of how the microspheres interacted with the cement. Additionally, lithium nitrate was mixed in these samples to understand the effect lithium nitrate has on cement. For these test,

only three samples of a cement with only microspheres and three samples of microspheres and 5% lithium nitrate in cement were tested. After 28 days of hydration the samples were tested using micro indentation the results for these tests can be seen in Table 4.1. For the indentation test both samples of dried and wet cement were tested to see the impact that the drying process had on the mechanical properties.

Table 4.1. Young's Modulus and hardness values cured at ambient conditions

Design	Hardness (MPa)	Young's Modulus (GPa)
Dry with $LiNO_3$	56.83 ± 8.12	3.87 ± .142
Dry Microspheres	84.34 ± 19.12	4.73 ± .226
Wet with $LiNO_3$	37.54 ± 7.99	3.46 ±.212
Wet Microspheres	57.33 ± 4.26	6.68 ± .074

From Table 4.1 drying samples has a significant impact on the mechanical properties of cement. In the samples with lithium nitrate the harness increased and the Young's Modulus stayed relatively unchanged, showing that the drying process made the cement stronger while not effecting the elasticity of the samples. Then in the samples with only microspheres the hardness decreased and Young's modulus increased, meaning that the samples became weaker but behaved more elastically. These differences in drying effects showed how much can change when drying occurs so it was determined that all samples should be tested while still saturated to mimic what is seen the wellbore. This data also shows that the addition of lithium nitrate decreased hardness as well as decreased Young's modulus. Meaning that the cement with lithium nitrate is both weaker and more elastic, because of the effects that lithium nitrate has on cement chemistry. The lithium nitrate is working as a retarder and reacting with silica before reactions that form C-S-H interact with the silica. Because the lithium nitrate is preventing this reaction it would also be assumed to prevent the ASR reactions with the microsphere because this is a similar reaction to C-S-H, and

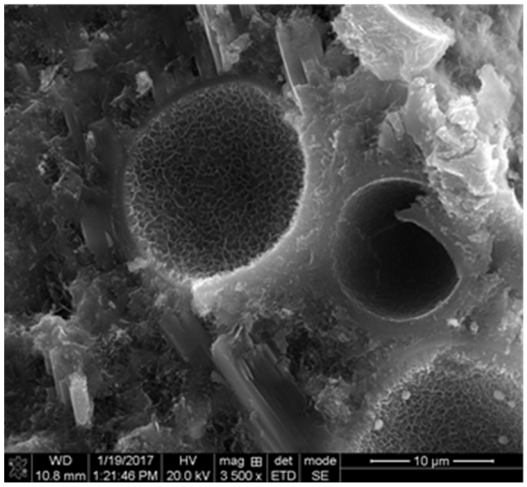	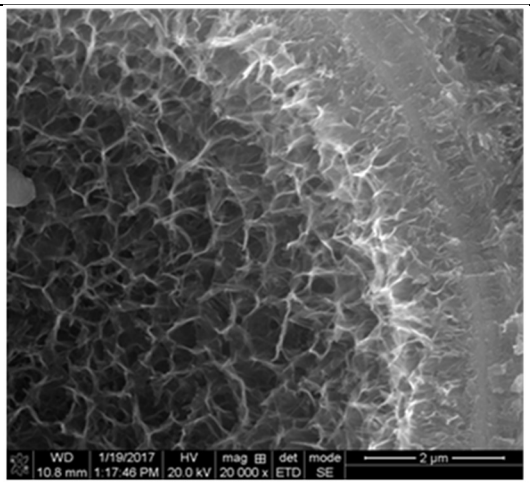
A. SEM images of reacted microspheres in the cement matrix with no preventative additives. The microspheres have reacted with the pore fluid and form a C-S-H and ASR layer as the wall reacts.	B. SEM image of only the microsphere wall from image above. Clearly seeing what is left of the wall and the ASR forming under the C-S-H
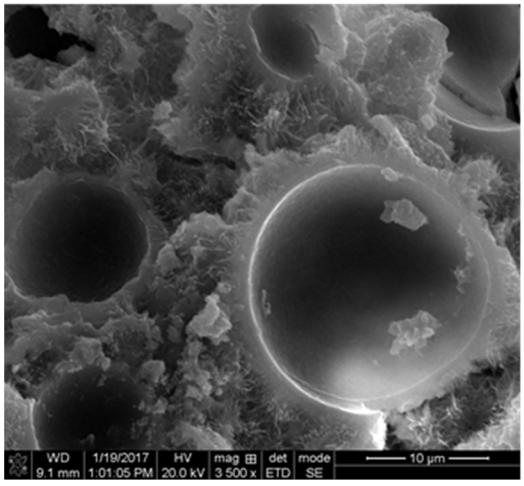	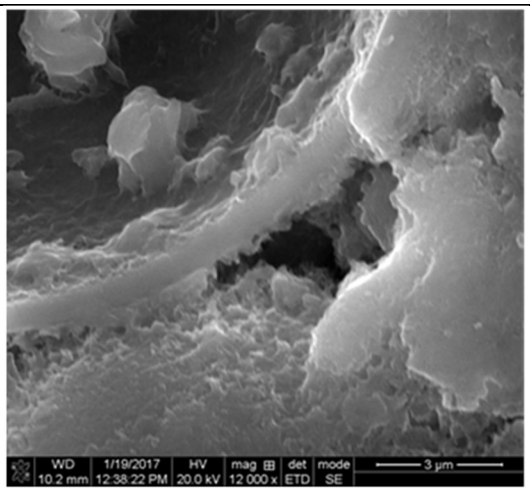
C. SEM images of microspheres in cement matric that have lithium nitrate mixed in. Microspheres are still intact with minimal interaction with cement.	D. SEM image of microsphere wall from above image showing almost no reaction with the cement

Figure 4.4 SEM images of microspheres in the cement matrix curried at ambient temperatures

C-S-H would typically form along the microspheres before ASR. This effect can be seen in the SEM images in Figure 4.4, where the samples with lithium nitrate have almost no reaction with the cement matrix. While the microspheres in the samples without lithium nitrate reacted with

the cement matrix causing almost none of the microphase wall to still be intact, instead leaving what appears to be a C-S-H and ASR gel layer forming in its place. These effects allowed for further interest in prevention of ASR as well as effects lithium nitrate have on this prevention.

4.3.1 Porosity Analysis

All mix designs were tested for porosity by measuring three different samples using a Helium Gas Porosimeter. The mean values of these test are shown in Figure 4.5.

These porosity values show that metakaolin and fly ash significant lower the porosity of these samples. Metakaolin was the most influential, dropping porosity by more than half from the samples with no preventive additives. Larger percentages of metakaolin do not result in significant changes in the porosities of the samples. Whereas, higher percentages of fly ash resulted in additional porosity drop. Both lithium nitrate and silica flour show little to no change on the porosity of the sample compared to the samples with no additives. These changes can be explained in that the metakaolin and fly ash are acting as SCM in the early life of the cement hydration forming more C-S-H and closing pore space. This extra C-S-H development leads to ASR prevention latter in the life of the cement because the reactants that cause ASR are already locked up in this C-S-H. Lithium nitrate acts a retarder in the cement matrix preventing C-S-H development in the cement and lower porosity. The silica flour used can be interpreted as an amorphous silica that acts the same as microspheres and allowing for the onset of ASR.

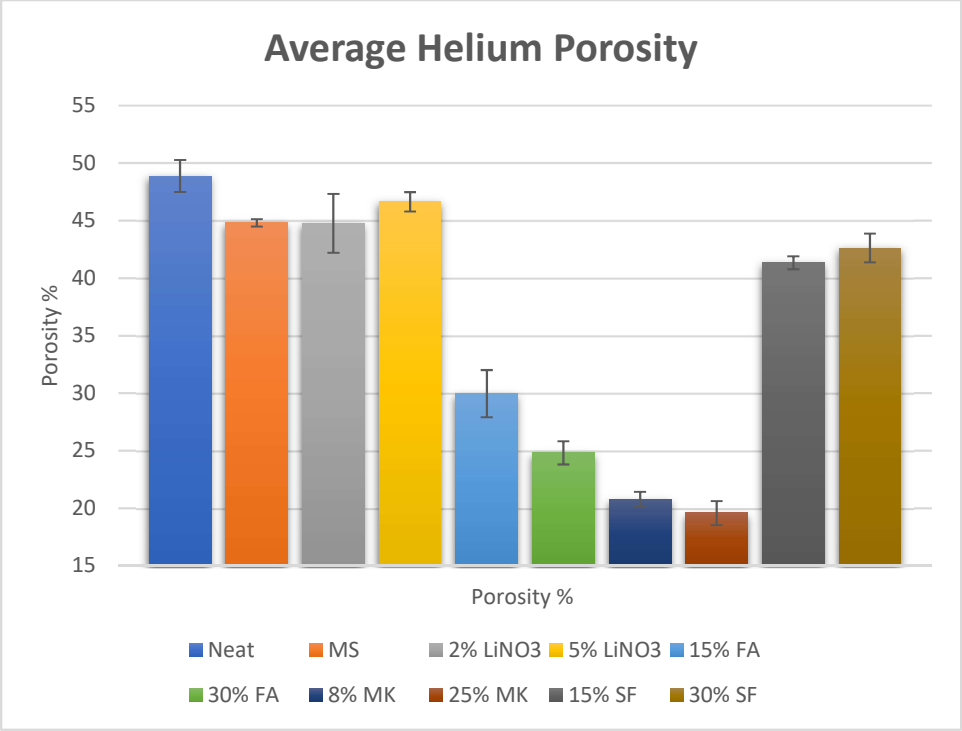

Figure 4.5: Graph showing the changes to average helium porosity values after one month of curing at 70ºC (158ºF) of dried samples. Showing that lithium nitrate and silica flour additive in the cement have little change on the dried porosity, and fly ash and metakaolin have large effects on the dried porosity of the samples. Error bars are showing standard divination of samples.

4.3.2 Permeability Analysis

Permeability measurements were taken on three samples from each mix using a liquid pulse decay permeameter. DI water was used to apply the pulse pressure in all test. The mean values of the three samples tested are shown in Figure 4.6. Value shown for the sample with only microspheres is from one test because two of the samples were destroyed during the testing prosses.

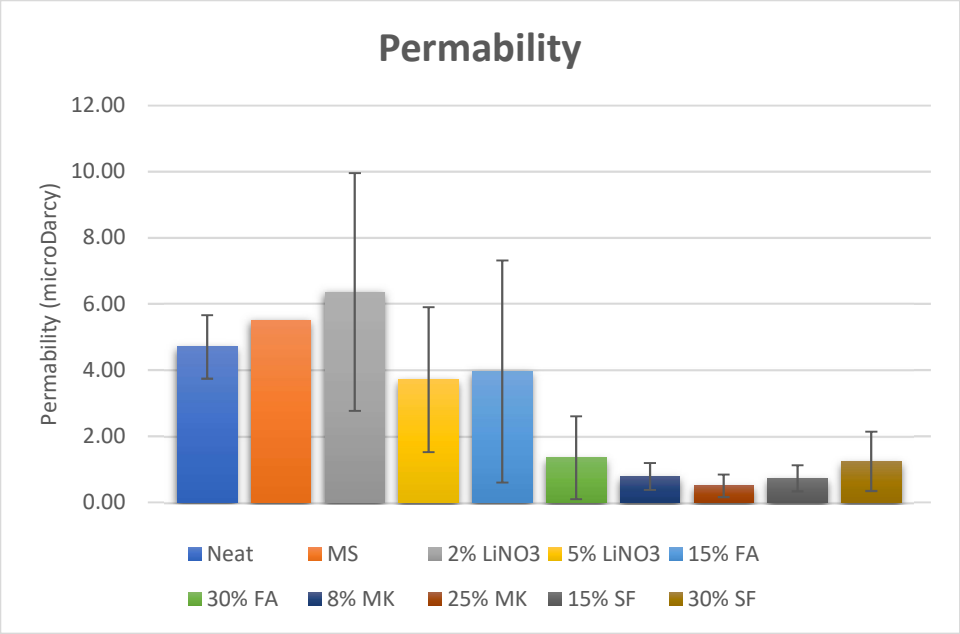

Figure 4.6: Graph displaying the average permeability of three samples tested using pulse decay permeability after samples were cured for one month at 70ºC (158ºF). Trends show that all additive lower permeability except low percentages of lithium nitrate. Silica flour fly ash and metakaolin have the largest impact on decreasing the permeability. Error bars shown are standard deviations.

Permeability values tested have reality large standard deviations because of the preciseness this machine. Because the machine can test the difference on the Nano Darcy scale, even the smallest imperfections in the cement cores will result in large differences. Still though trends in the permeability changes can be seen. All additives appear to be lowering the permeability of the cement, besides lithium nitrate. Again, lithium nitrate inhibiting the growth of C-S-H means that more pore space will be open and allow for flow. Then all other additives are working as pozzolanic materials and leading more C-S-H growth closing off space for fluid to move through. Metakaolin and fly ash appear to have the largest impact on lower cement permeability.

4.3.3 Indentation Mechanical Properties Analysis

Micro indentation was performed on all mix designs after curing. For this ten indentation marks were mad on a flat surface of a core. Three cores were tested like this and then all values were averaged together to come up with mean Young's Modulus and Hardness for each design. These values can be seen in Figure 4.7.

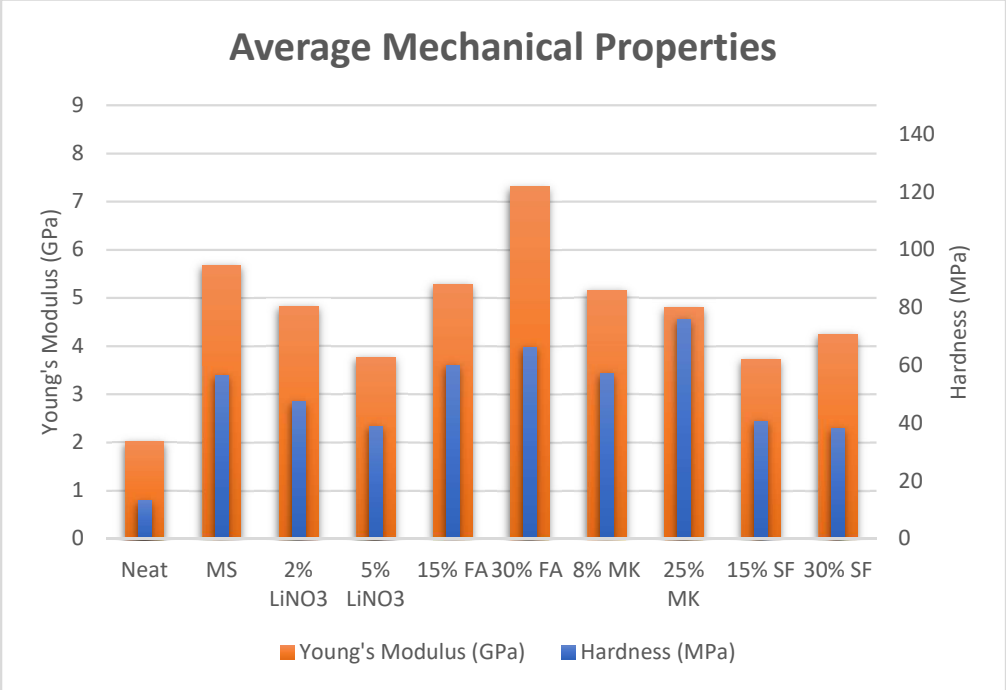

Figure 4.7: Graphs showing changes in Young's Modulus and hardness taken from micro indentation testing. Values shown are averages of ten indentations on three different samples from each design after being cured for one moth at 70ºC (158ºF). All additives show an increase in hardness and Young's Modulus compared to neat. Trends show hardness increasing in all samples besides silica flour and lithium nitrate when compared to only microspheres. Young's modulus changes are not as large with lithium nitrate and silica flour increasing elasticity and metakaolin and fly ash not having large impacts expect low percentages of fly ash decreasing elasticity as compared to microspheres.

Interpreting these values needs to be broken up by each additive and compared back to only microspheres. Lithium nitrate lowered both the Young's Modulus and the hardness with high mix percentages lower both even further. Metakaolin at lower mix percentages did not affect Young's modules and Hardness, while high mix percentages lowered the Young's Modulus and increased the hardness. Silica flour lowered the Young's modulus with a high mix percentage

lowering the value less, and increasing mix percentages increased the hardness loss. Fly ash acted like metakaolin not changing much at low mix percentages but having a more significant increase in Young's modulus and hardness at high mix percentages.

4.3.4 Microstructure Analysis

Optical images were taken for the dried samples only containing microspheres to see if it was possible to see signs of ASR development at low magnifications. These images can be seen in Figure 4.8 and show cracking connecting microspheres indicative of ASR formation and not from the drying process.

SEM images were also taken of dried samples of each mix design to visualize microspheres interactions with the cement. These images can be seen in Figure 4.9 comparing each additive to a sample with no additive. Each additive has two images from the larger mixture percentage samples, an image at high magnification of the microsphere in the cement matrix, then a higher magnification image of the microspheres wall to see how much of the wall is still unreacted.

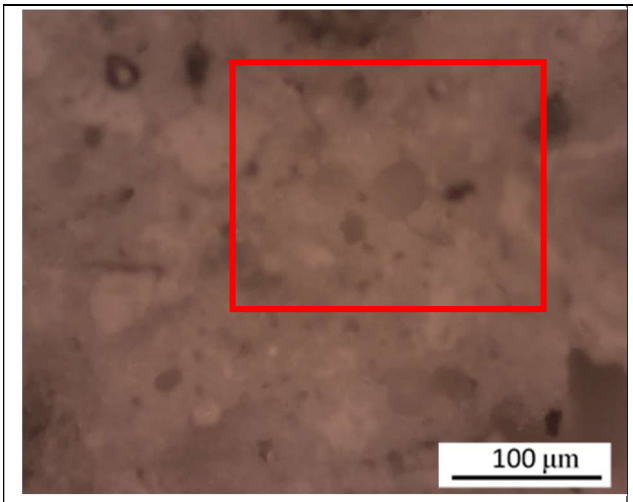	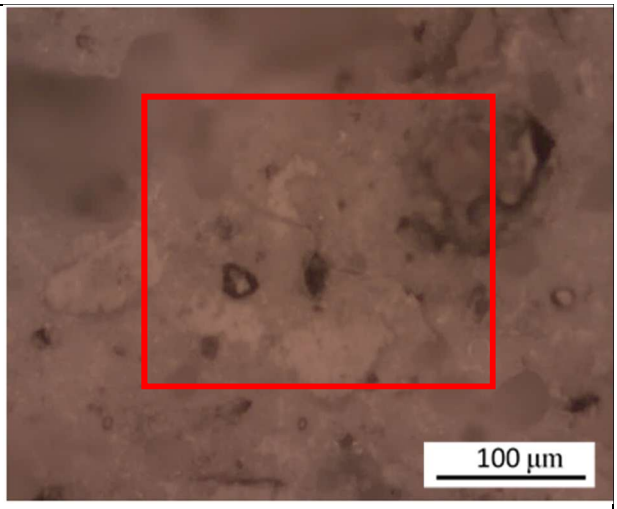
A. Optical image at low magnification sowing crack in surface of cement contesting along a path on the edge of microspheres, hinting at the onset of ASR. Crack is inside red square.	B. Second sample showing optical image with a crack starting from the outside of a microsphere, hinting at ASR

Figure 4.8: optical images from cement samples containing only microspheres post curing showing cracks hinting at ASR formation

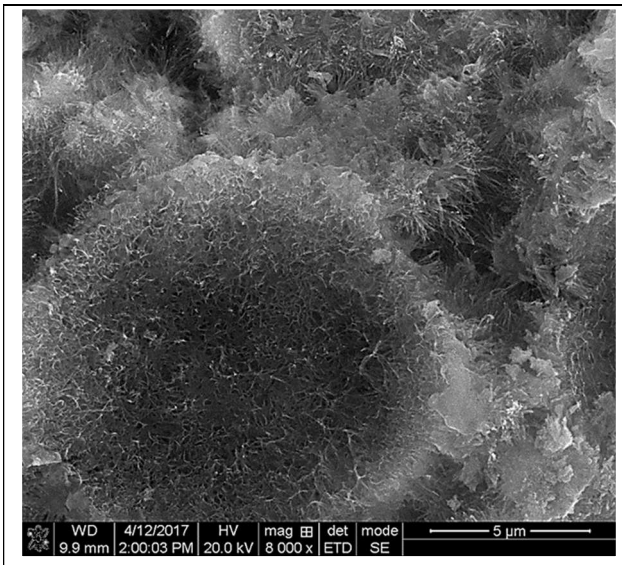	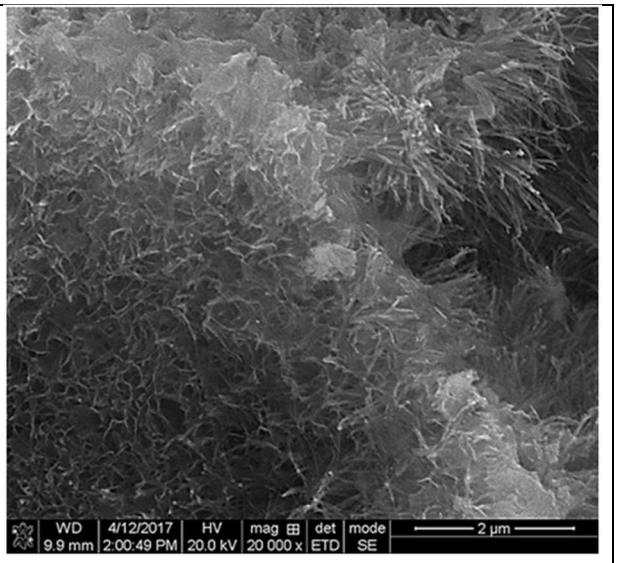
A. SEM image from sample with no preventive additives after being cured. Microsphere has completely reacted with cement pore fluid leaving almost no microsphere wall only a layer of C-S-H with ASR growing underneath	B. SEM at higher mag than image above showing what is left of the microsphere wall with only C-S-H and ASR remaining

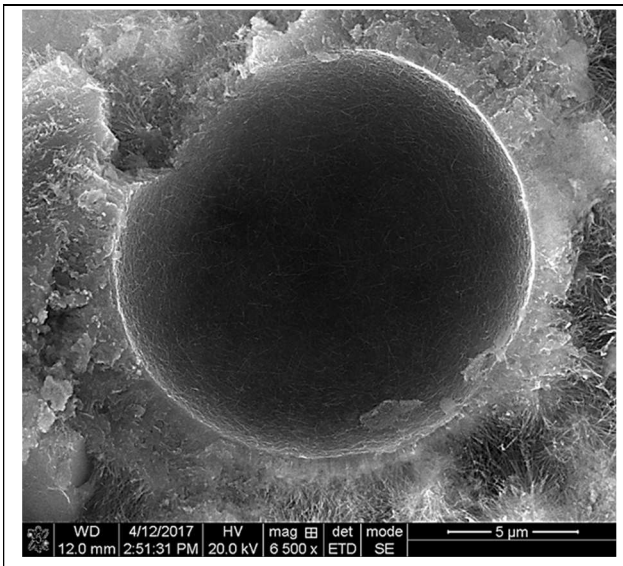	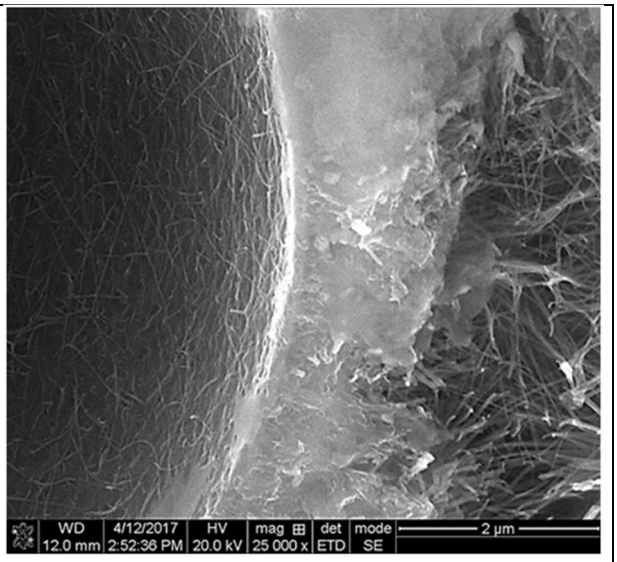
C. SEM image from sample with 5% lithium nitrate after curing. The microsphere wall is still intact with almost no reaction occurring with the wall	D. SEM image at higher mag from image above with 5% lithium nitrate. Showing no reaction with the microsphere wall and the cement matrix. Some crystal structure on the surface showing lithium silica barrier
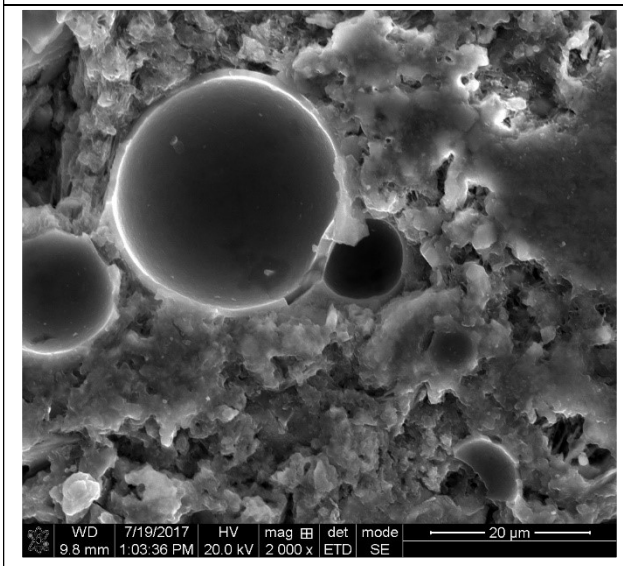	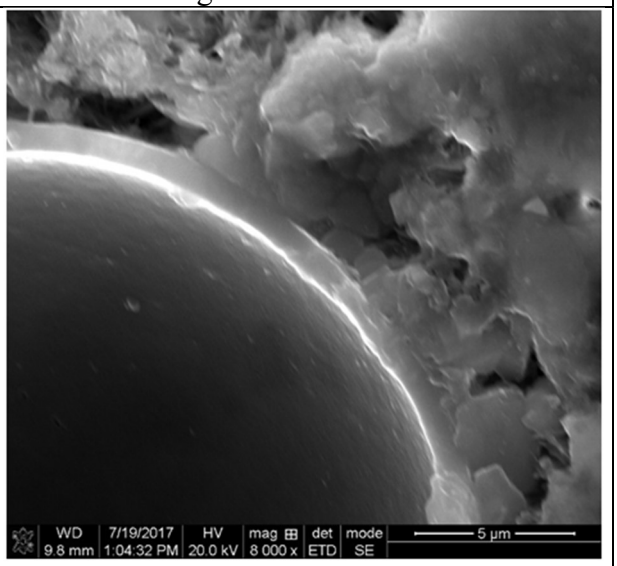
E. SEM image from sample with metakaolin after curing. No reactions appear to be happening with the microsphere wall keeping the wall intact.	F. SEM image at high magnification of microsphere with metakaolin. No reaction has occurred with the microsphere, resembles microsphere from manufacture

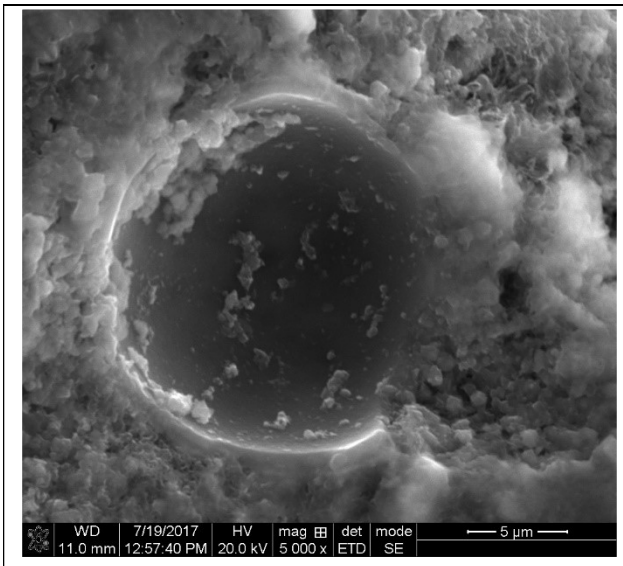	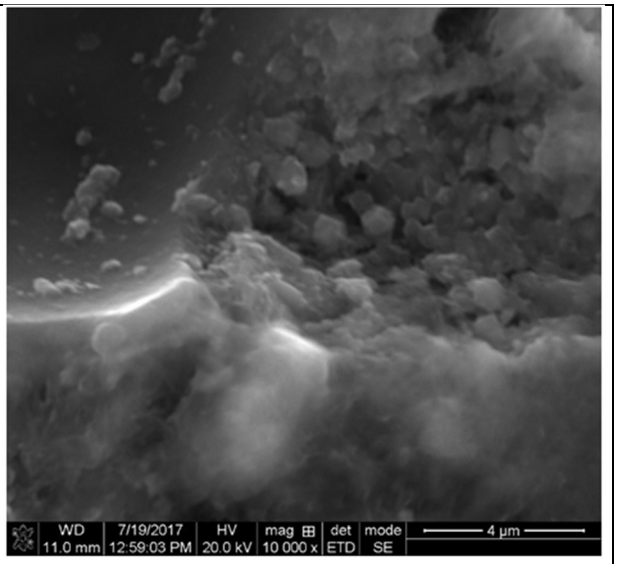
G. SEM image from sample with fly ash. Microsphere in the cement matrix after curing and no reactions appear to be happening with the microsphere wall keeping the wall intact. Appears to be some interaction with surrounding matrix.	H. SEM image at high magnification of microsphere with fly ash. No reaction has occurred with the microsphere, resembles microsphere from manufacture except some interaction on outside wall with cement matrix
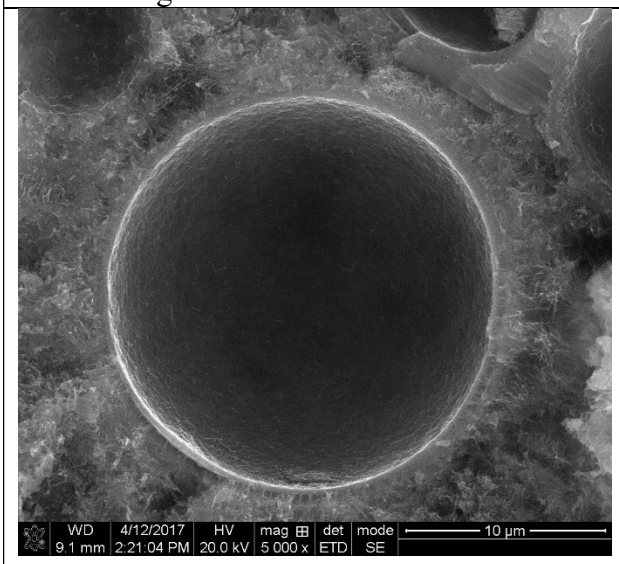	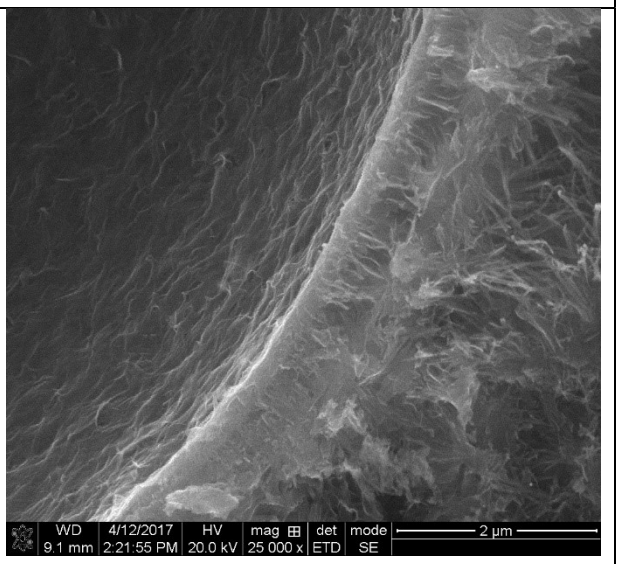
I. SEM image from sample with silica flour after curing. Reactions are starting to occur with the microsphere and a C-S-H like structure starting to form but not as reacted as sample with no additives.	J. SEM image of microsphere wall with silica flour additive after curing. Can be seen that the wall is starting to react with matrix but not fully reacted.

Figure 4.9: SEM images of microspheres in cement cured at 70ºC (158ºF) with different admixtures showing various reactions

4.4 Additional Microscopy Data

In addition to SEM, backscatter images were also taken on a sample containing 30% metakaolin to investigate if this is an effective method in distinguishing the differences in composition between C-S-H, the microspheres, and ASR. High magnification and low magnification backscatter images of samples can be seen in Figure 4.10. From these images, the microspheres are much darker than the C-S-H structure showing that the microspheres have a lighter composition.

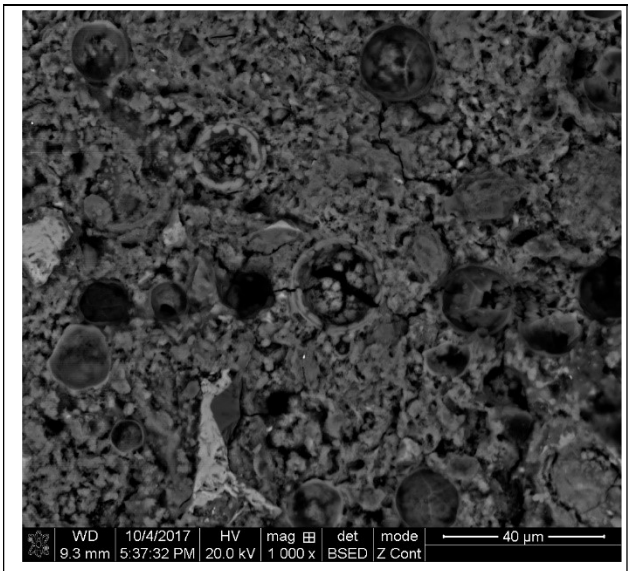

High magnification backscatter SEM image of microspheres in cement matrix. Microsphere are clearly distinguishable between C-S-H matrix.

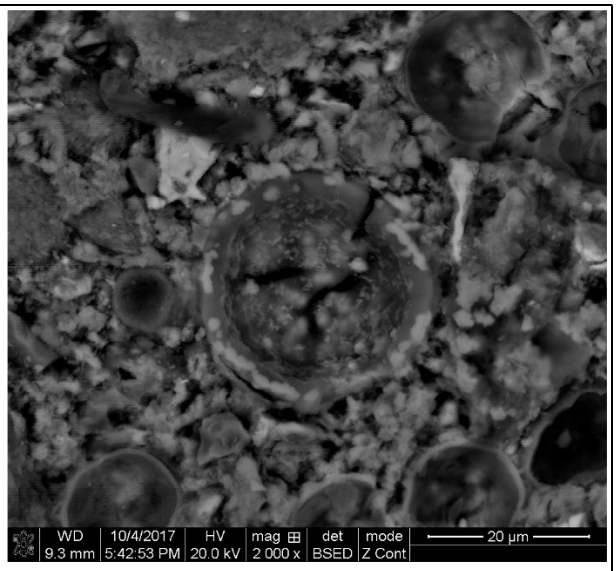

Low magnification backscatter SEM image of microspheres in cement matrix. Microsphere wall is lighter and clearly destructible differences from the C-S-H matrix.

Figure 4.10: Backscatter SEM images of microspheres in cement cured at 70ºC (158ºF) with metakaolin additives into the cement

EDS was also conducted on this sample containing 30% metakaolin so see changes in the chemical ratios in the cement starting from the center of the microsphere and moving out into the cement matrix. These results can be seen in Figure 4.11. From these spectrums, it can be noted

that there is not any oxygen along the edge of the microsphere showing that the SiO_2 has been broken down and only leaves the silica to react with calcium which is at a high Ca:Si ratio. Also, a small amount of aluminum is present because aluminum is a large percentage of metakaolin. This also resembles what is seen out in the C-S-H with all ratios almost the same. Chromium also appears to be present but is assumed to be a false reading for iron that can be present in cement. Then inside the microsphere oxygen in preset showing that SiO_2 is still intact but there is also iron and Aluminum from the metakaolin as well as calcium showing some reaction going on with the microsphere wall that resembles C-S-H but the microsphere wall is still intact.

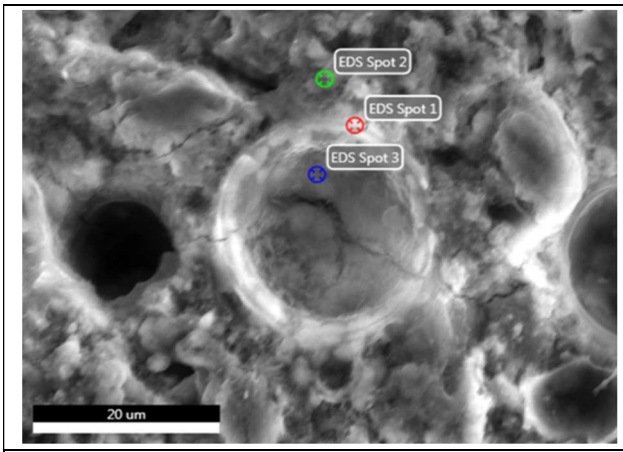

EDS Spot 1

Element	Weight %	Atomic %
Al	.93	1.3
Si	14.63	19.68
Ca	81.87	77.16
Cr	2.57	1.87

EDS Spot 2

Element	Weight %	Atomic %
Al	.8	1.12
Si	14.43	19.43
K	.21	.2
Ca	82.16	2.18
Cr	2.18	1.58

EDS Spot 3

Element	Weight %	Atomic %
O	13.14	26.75
Al	3.37	4.07
Si	12.17	14.12
Ca	66.06	53.71
Fe	4.81	1.2

Figure 4.11 Shows EDS spectrums of how the chemical composition changes around the microsphere from the center of the microsphere out the wall of the microsphere and then in the C-S-H of the cement matrix for samples containing 30% metakaolin and microspheres in cement cured at 70ºC (158ºF)

4.5 Expansion Study Results

To see if any expansion could be noted visually in the lab samples with and without microspheres were monitored in graduated cylinders. Both the cement levels and the water levels were recorded periodically over three months. The values for the water levels can be seen in Table 4.2, as well as Figure 4.12 shows visually the starting to ending setup of the sample with microspheres. The water levels dropped much more significantly in the samples with the microspheres than in the samples without. The values for cement levels never changed more than 1 mL on the graduated cylinder, but the samples with microspheres were moving closer to gaining 1 mL, while the samples without microspheres were close to losing 1 mL. Since this was a visual test these numbers cannot be quantified so they are not presented, but this shows that expansion with microspheres and shrinkage without them. Also, the increasing loss of water supports the idea that the microspheres were absorbing the water like what would be expected with ASR.

Table 4.2: Expansion test results change in water level. Values shown are the water level reading in the graduated cylinders, numbers shown are the average of three test

Design	0 Weeks	2 Weeks	4 Weeks	2 Months	3 Months
Microspheres	50	42	42	41	40
Clean	50	48	47	47	46

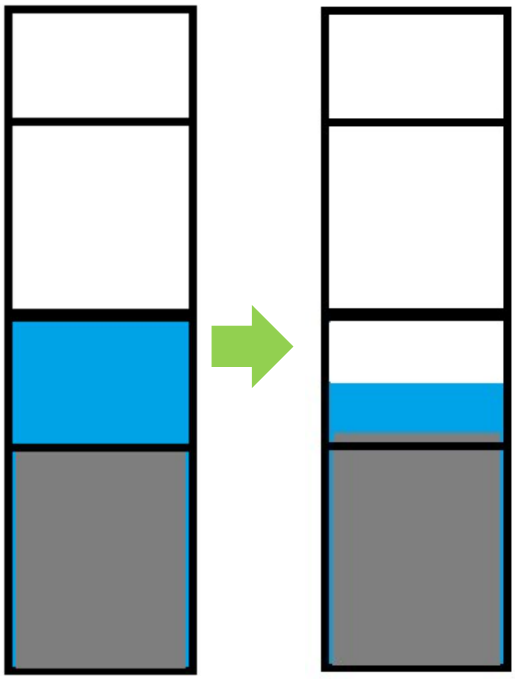

Figure 4.12: Graphic of how the sealed graduated cylinders changed from the samples with microspheres, with the water levels and cement level starting on distinguishable lines. After two weeks, the water had clearly been absorbed into the cement and the cement had risen above the line it started on.

CHAPTER 5: DISCUSSION

5.1 Mechanical and Petrophysical Property Analysis

This study investigated multiple different mechanisms for ASR prevention with silica-based microspheres in wellbore cements. These methods all had effects on the mechanical and petrophysical properties of the cement. Figure 5.1 shows the percent change of the different sample types in comparison to neat cement samples. This figure illustrates that as the water/solids ratio decreases, the respective samples increased in hardness and Young's modulus while conversely decreasing in permeability. This trend is likely due to the additional C-S-H growth.

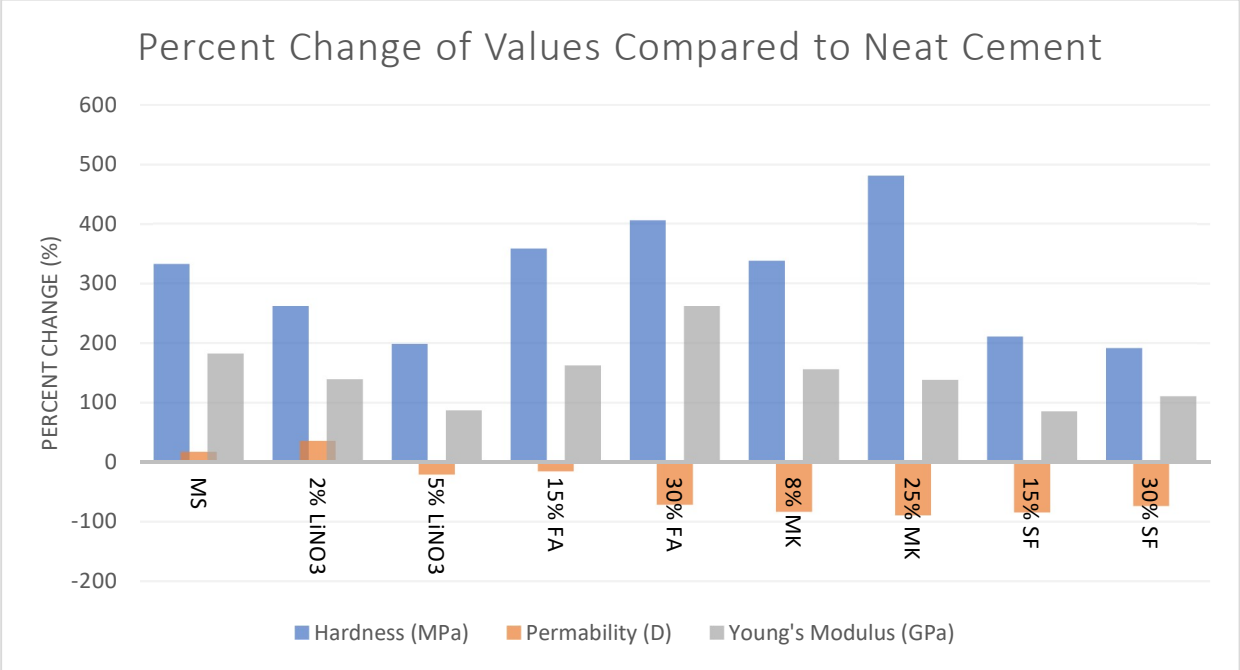

Figure 5.1: Percent change of Hardness, Permeability, and Young's Modulus values compared to neat cement samples of the same density. Shows a uniform increase in Young's Modulus a hardness because cement has a lower water percentage with microsphere addition and an almost uniform decrease in permeability because of lower water rate and more C-S-H growth.

Figure 5.2 then shows a comparison of mechanical and petrophysical properties of samples containing only microspheres to those containing microspheres and lithium nitrate, fly ash, or silica flour. This comparison shows the changes additives intended to prevent ASR, have on the cement containing microspheres.

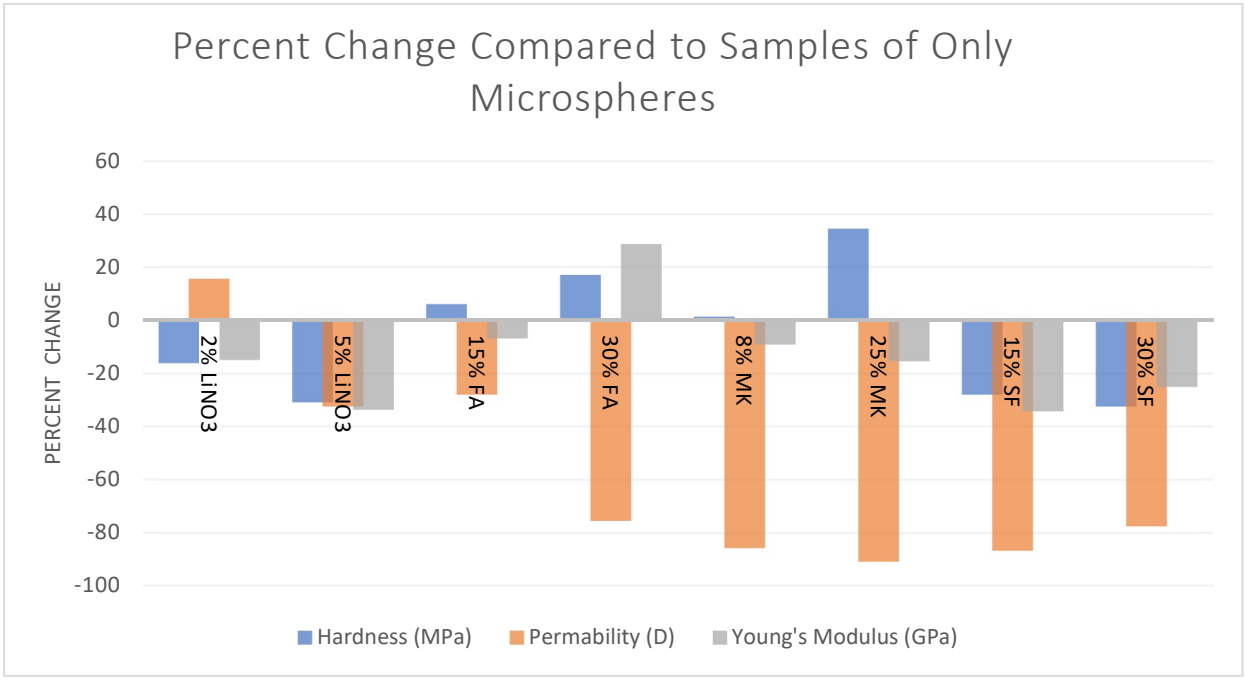

Figure 5.2: Comparison of Hardness. Young's Modulus, and permeability of samples showing percent change compared to only microspheres to see effects of different additives. Showing how metakaolin and fly ash increase Young's modulus and hardness while all other additives decrees this. While almost all additives decrees permeability.

As was displayed in the SEM imaging, fly ash, metakaolin, and lithium nitrate were successful at preventing ASR while silica flour was not. Silica flour does not prevent ASR because the silica is in an amorphous state but is not highly reactive, so the silica does not react with the pore fluid during hydration instead reacting latter on like the microspheres creating more C-S-H and ASR. Metakaolin and fly ash work in similar fashions by reacting early in the cements' hydration to form excess C-S-H, so there is little alkalinity latter in the cement pores to react with

the microspheres. The lithium nitrate on the other hand works at preventing ASR by acting like a retarder and bonding with the silica in the cement matrix and cutting off further reactions with the silica, as well as reacting with the OH^- and lowering the alkalinity of the cement. Lithium nitrate both prevents the growth of C-S-H early in the life of the cement, but also prevents ASR reactions latter in the cement life.

Evidence of how these additives work is seen in the petrophysical properties as well. Where lithium nitrate and silica flour did not affect the porosity, whereas metakaolin and fly ash decreased porosity. Then for permeability, lithium nitrate increased the permeability at low mixture percentages and decreased the permeability at high mix percentages. Whereas metakaolin, silica flour, and fly ash all lower the permeability. Fly ash, silica flour, and metakaolin are increasing C-S-H development in the cement so there is less pore space present leading to lower porosity and permeability. The silica flour is also acting in the same way the microspheres do reacting with the cement and forming some C-S-H and ASR, this ASR gel formation is decreasing the permeability. And with lithium nitrate acting as a retarder C-S-H development is halted allowing for more pore space therefore increasing permeability.

Changes in mechanical properties can be seen effecting both the hardness and Young's modulus values. With Silica flour and lithium nitrate less C-S-H development leads to less strength development seen in lower hardness values. While metakaolin and fly ash both lead to more C-S-H development allowing for more strength and a higher hardness value. The same trend can be seen with Young's Modulus values where the lower strength also leads to more elasticity, and more strength making the material less elastic except in the case of metakaolin. Metakaolin has a higher aluminum oxide content than fly ash, that in the cement matrix also leads to the formation of more ettringite which will allow the matrix to absorb more water making the cement

more elastic. This trend can be seen in other metakaolin studies where cements with metakaolin absorbs more moisture than those with fly ash (Mobili 2016).

Previous studies on lithium nitrate in cements have shown that the inclusion of lithium nitrate in cement inhibits the growth of C-S-H (Milliard and Kurtis 2007). This trend is also seen in this study with the loss of mechanical and petrophysical properties being attributed to less C-S-H growth. Though lithium nitrate is effective at inhibiting ASR development, this loss of strength and higher permeability makes for a cement that is less effective at suppling proper zonal isolation and strength. For these reasons individual test should be conducted to interoperate if lithium nitrate is an acceptable ASR prevention mechanism for that individual well.

This study and previous studies have shown that both fly ash and metakaolin are effective at preventing ASR, increasing mechanical properties, and decreasing porosity and permeability. This is because both materials act as SCM creating pozzolanic reactions and creating more C-S-H (Snellings, Mertens, and Elsen 2012). The differences between these materials come in their composition. Both are mostly amorphous silica that will react like cement and form C-S-H, but metakaolin is around 40% aluminum oxide whereas fly ash has around 15% aluminum oxide. These differences lead to differences in the cement composition that can affect the cement latter in the life span of the cement. Other studies have also shown that metakaolin and fly ash are working in similar ways with metakaolin being able to function at lower mix percentages (Moser 2010) (Shen 2017).

With silica flour, this study showed not much change with how the cement acted with and without the silica flour. This is because the silica used acts like the silica in the microspheres and though it holds up through the initial cement reactions the silica flour reacts latter and leads to

more on set of ASR. Previous studies on silica flour in wellbore cements showed a similar reaction going on with the cement pore fluid (Bello et al. 2014).

This study can also be compared to another study conducted by Haliburton on microsphere stability at high temperatures and pressures after 5 days of curing A comparison between total microspheres reaction in the Halliburton study and from this one can be seen in Figure 5.3. These two images show similar reaction mechanisms where nothing is left of the microsphere wall but the ASR gel and some C-S-H. This helps support that the reactions seen in this study are ASR. Also, the Haliburton study also looked at many different silica compounds to prevent this reaction with the microspheres in the short term and show fly ash at having positive results for prevention of these ASR reactions (Santra and Luo 2016). It should be noted that there are differences between this study and the Haliburton one mainly in that the Haliburton one was conducted at much higher temperatures, this leads to changes in the structure of C-S-H that are less stable (Meducin et al. 2006).

Another study performed on microspheres at similar temperatures as this study, but at much higher pressures showed no shrinkage (Al-Yami 2008). That study also showed the ability of cements containing microspheres to perform in field conditions and can provide proper structural strength and zonal isolation. That study showed SEM images of microspheres reacting in these field conditions and being destroyed forming ettringite and ASR. Though ettringite formation was not shown in this study both ASR and ettringite lead to expansion later in life of the cement as water is absorbed (Mehdi et al. 2017). This expansion can lead to cracking effecting the integrity of the cement.

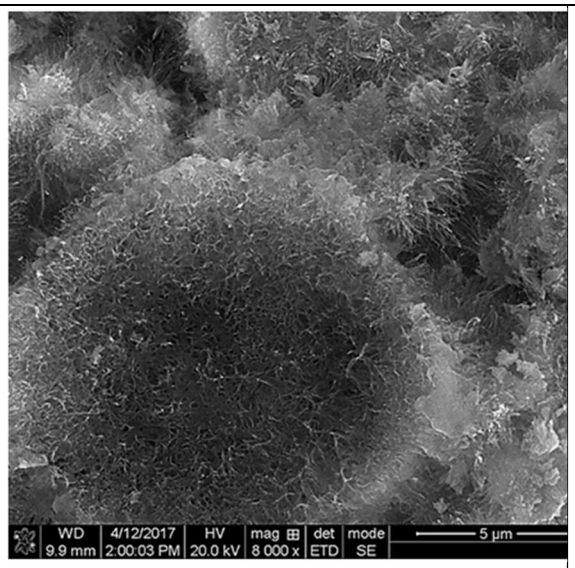

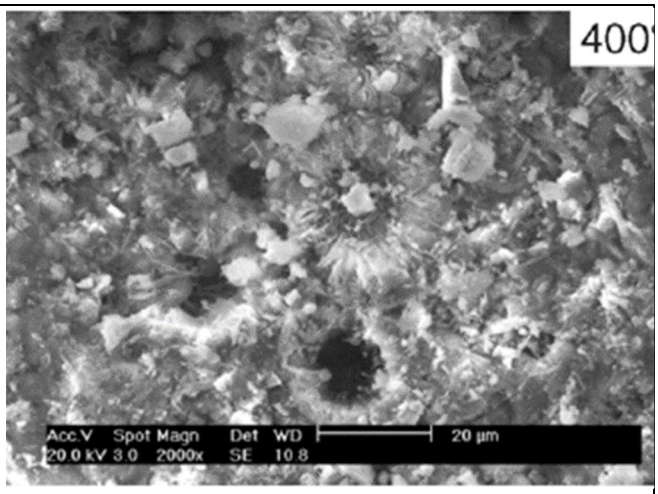

A. SEM image of microsphere taken from this study. Cured for 28 days at 70ºC (158ºF). Showing total microsphere reaction with the cement matrix leaving only ASR	B. SEM image from Halliburton study showing. Cured for 5 days at 205ºC (400ºF). Showing complete microsphere reaction with the cement and leaving only ASR. (Santra and Luo 2016)

Figure 5.3: Two SEM images from two different studies on microspheres, this one and one by Halliburton. Both images show similar break down reactions of the microspheres and leaving only ASR.

5.2 ASR Expansion Analysis

In addition to understanding ASR prevention with the use of microspheres it was also needed to understand how these cements would expand as ASR formed. From the ASR expansion study, it was seen that without microspheres cement shrunk somewhere between 1 to 4%, this value is within the range presented by (Nelson and Guillot 2006) of .5 to 5% bulk shrinkage of Portland cement. This shrinkage is expected in most every wellbore cement and can lead to issues such as sustained casing pressure as the cement and casing debond during this shrinkage period. Because of shrinkage issue in cements the fact that microspheres are leading to a 1 to 4% expansion in the same time frame that typical Portland cements shrunk, could lead to possible positive

outcomes with no debonding between the cement and casing. Over longer periods of time and different types of silica content expansion can lead to high amounts of strength loss. As the ASR gel forms, it absorbs more and more water. This absorption of water was seen in this study where the sample with microspheres absorbed much more of the confining water than the sample without microspheres. This absorbed water leads the ASR expansion and the eventual cracking of the cement and loss of tensile strength. This loss of strength can be seen in many other studies that have been conducted looking at impacts of ASR on cement expansion and strength. One study looking at microspheres in class H cements (Sabin 2005) sowed a similar trend of shrinkage in cements without microspheres and expansion with microspheres, while at the same time having a loss of around half of the cements compressive strength in the samples with microspheres. That study was conducted at similar temperatures as this one and run for a longer period of time but show similar results, verifying the need to prevent ASR in cements containing microspheres. Additional studies have been conducted over the years investigating ASR in concretes for construction purposes. These studies also show the same trend where expansion is also accompanied by loss in strength of the concretes (Justnes 2016) (Markouk 2003).

Wellbore integrity issues are something that have long plagued the oil and gas industry. Bad cementing can lead to an onslaught of different wellbore integrity issues that can lead to micro annular gas flow allowing gas to flow through or around the cement (Bonett and Pafitis 1996). One of the ways these pathways form to allow gas flow is through cement shrinkage. A 1% volumetric shrinkage of the cement can lead to micro annular gaps of around 1.7 micros and allow for an additional 240 mD of flow through the cement (Kupresan et al. 2014). Figure 5.4 shows how cement shrinkage allows for a gap to form on the outside of the cement allowing fluids to flow up the wellbore, but by preventing shrinkage this flow can also be prevented. Using these

microspheres and controlling the expansion of cement could counteract shrinking and prevent gas flow around the cement. In the past expandable cements have been used to try to accomplish these goals (Seidal and Greene 1985), but these techniques were not good for the long-term stability of the cement because of negative interactions within the cement undergoing sulfates attack from the sulfates used for expansion. Using microspheres as seen in this study, ASR could be allowed to form and expand to prevent debonding of the cement in balance with other additives that could be used to cut off the ASR reaction before total loss of cement strength and integrity.

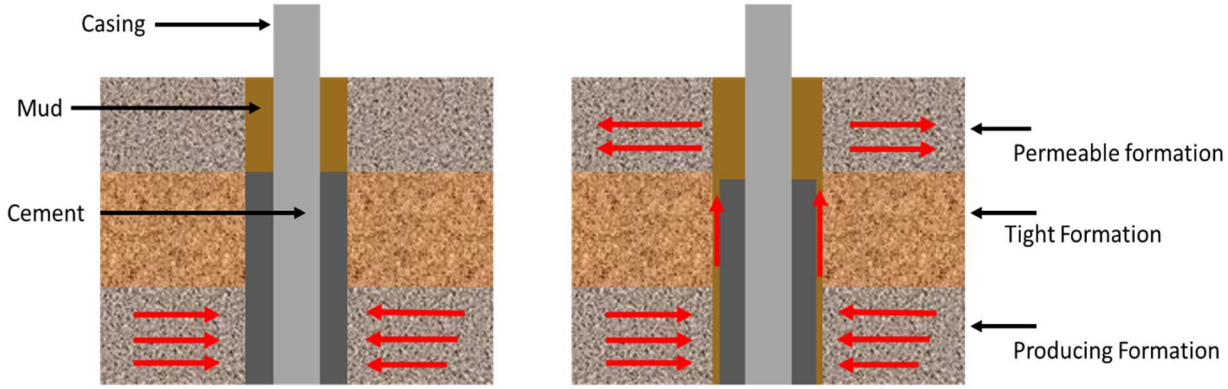

Figure 5.4: Shows how on the left as the cement shirks a microcannulas is formed around the cement allowing for fluids to flow up the wellbore, but by preventing this shrinkage as seen on the right flow up the wellbore is cut off because there is no microcannulas.

One thing this study exemplified is that cement is a complex structure that should not be simplified and assumed what worked once will work again. The effects of lithium nitrate and microspheres where drastically different when cured at temperature when compared to being cured at ambient conditions. Then small changes of mix percentages of some additives can have large changes in properties of the cement sometimes but small changes other times. For this reason, every cement job needs to be designed and fit to purpose for what each well will be experiencing throughout the lifetime of the well. It should also be noted that microspheres are not the only

source of reactive silica used in wellbore cements. Many additives have silica in them that is non-reactive in acidic solutions, the same may not be the case with basic solutions in cements. An extensive literature review was conducted on ASR, and showed that every component of cement and concrete can have an influence on the reactivity with the cement from silica type and size, to temperature and pressure, to presences of salts (Lindgard 2012). For these reasons, every cement should be tested for the life of the well before the cement is run.

5.3 Wellbore Integrity Time Line

Inspecting issues happening throughout the life of a well and the operation of the well, a well integrity time line can be formed. This time line is seen in Figure 5.5, showing that a well starts in a design phase, then goes into drilling and completions, then operation, and finally plug and abandonment. At any point in this time line issues can arise negatively impacting the wellbore integrity, that eventually all need to be addressed during the plug and abandonment phase where the well must be permanently sealed. Because of this all phases of the well life must be considered during the planning part of the well not just the drilling and completions portions to minimize safety, environmental, and financial issues throughout the life of the well.

Figure 5.5: Well integrity life line showing show how the design portion of a well must address all other portions of the well life

CHAPTER 6: CONCLUSIONS AND RECOMMENDATIONS

6.1 Conclusions

This study investigated and tested the presence and effects of ASR in lightweight wellbore cements containing silica-based microspheres. After an understanding of these effects were developed ASR prevention mechanisms were also tested for potential effectiveness.

Silica-based microspheres, are alkali active and will react with the cement pore fluid leading to the onset of ASR. This reaction happens faster at higher temperatures and can be affected by additives in the cement. ASR forms along with C-S-H during this process but ASR ends up controlling the reactions and leading to expansion and cracking as microspheres are completely reacted.

Fly ash and metakaolin are both effective at preventing ASR reactions while increasing mechanical properties and decreasing petrophysical properties. Lithium nitrate will prevent ASR but negatively effects mechanical and petrophysical properties. Silica flour acts like the microspheres and leads to ASR.

Because ASR is forming some expansion is occurring and counteracting the bulk shrinkage expected in cement.

6.2 Recommendations

Future work on this topic should look at longer time frame studies. ASR is a slow reaction and take long times to fully show the effects that come with it. This study invested aged these effects over 28 days. In the field, these cements will be expected to form over 30+ years so this 28-day time frame shows very little of the cement life.

Many other factors can affect ASR, more test could be run to test these factors. These factors could be: silica partial size and percentages, pressures, more temperatures, and contacts to salts. The additives tested in this study are also not the only ASR prevention mechanics so these could be tested in these different environments.

Additionally, larger scale lab test could be run on controlling ASR as a method to prevent microannular gas flow with cement bond interactions and running gas flow experiments. These experiments would focus on controlling the expansion reactions to prevent gas flow while still holding required cement strength.

REFERENCES

1. Abdullah, M. N., Bedford, D., Wong, S. R., & Yap, H. S. (2013, October 22). Prehydrating High-strength Microspheres in Lightweight Cement Slurry Creates Value for Offshore Malaysian Operator. Society of Petroleum Engineers.
2. Alessandra Mobili, Alberto Belli, Chiara Giosuè, Tiziano Bellezze, Francesca Tittarelli. (2016) Metakaolin and fly ash alkali-activated mortars compared with cementitious mortars at the same strength class, Cement and Concrete Research, Volume 88, 2016, Pages 198-210.
3. Al-Yami, A. S., Nasr-El-Din, H. A., Al-Arfaj, M. K., Al-Saleh, S., & Al-Humaidi, A. S. (2008, January 1). Long Term Evaluation of Low-Density Cement Based on Hollow Glass Microspheres Aid in Providing Effective Zonal Isolation in HT/HP Wells: Lab Studies and Field Applications. Society of Petroleum Engineers.
4. API 10B-2, Recommended Practice for Testing Well Cements, second edition. 2013. Washington, DC: API.
5. B. Fournier, M.-A. Bérubé, G. Bergeron, A rapid autoclave mortar bar method to determine the potential alkali–silica reactivity of St. Lawrence lowlands carbonate aggregates, Cem. Concr. Aggregates 13 (1991) 953–957.
6. Bello, Kolawole. Radonjic, Mileva. (2014). Geochemical Evaluation of Geopressured wellbore Cement. Article. Microscopy and Microanalysis 20(S3): 1136-1137. August.
7. Bonett, Art. Pafitis, Demos. (1996) Getting to the Root of Gas Migration. Oilfeild Review.
8. Brufatto, C., Cochran, J., Power, L.C.D., El-Zeghaty, S.Z.A.A., Fraboulet, B., Griffin, T., Munk, S., Justus, F., Levine, J., Montgomery, C., Murphy, D., Pfeiffer, J., Pornpoch, T., Rishmani, L., 2003. From mud to cement e building gas wells. Schlumb. Oil Field Rev. 15, 62e76.
9. Burton K. Under Water Group (2005) Structural integrity of North Sea Wells. Published in the Journal of Offshore Technology in May/June.
10. Carver, B., Fitryansyah, Y., & KP, B. A. (2011, January 1). Improving Heavy-Oil Well Economics with Hollow Microsphere Cementing Solutions: Case History. Society of Petroleum Engineers.
11. Chief counsel's report – Chapter 4.4: Foamed Cement Stability. National Commission on the BP Deepwater Horizon Oil spill and offshore Drilling.
12. Du, H., Carpenter, K., Hui, D., Radonjic, M. (2017). Microsturcture and Micromecechanics of Shale Rocks: Case Study of Marcellus Shale. Facta Universitatis, Series: Mechanical Engineering. Vol. 15 Issue 2, P331-340.
13. Dhir, Ravindra K., T. D. Dyer, and M. C. Tang. (2009) Alkali-silica Reaction in Concrete Containing Glass. Materials and Structures 42.10: 1451-462.

14. Duchesne, Josée, and Marc-André Bérubé. (2001) Long-term Effectiveness of Supplementary Cementing Materials against Alkali–silica Reaction. Cement and Concrete Research 31.7: 1057-063.

15. F. Meducin, H. Zanni, C. Noik, G. Hamel, B. Bresson, Tricalcium silicate (CS) hydration under high pressure at ambient and high temperature (200 °C), Cement and Concrete Research, Volume 38, Issue 3, 2008, Pages 320-324.

16. Fournier, Benoit, and Marc-André Bérubé. (2009) Alkali-aggregate Reaction in Concrete: A Review of Basic Concepts and Engineering Implications. Canadian Journal of Civil Engineering 27.2: 167-91.

17. Gieger, C., Fazio, J., Spaulding, R., Kutchko, B., & DeBruijn, G. (2016) Physical and Mechanical Properties of Field-Generated Foam Cements: Implications for Cement Property Prediction and Modeling. Society of Petroleum Engineers.

18. Goldstein, J., Newsbury, D., Joy, D., Lyman, C., Echlin, P., Lifshin, E., Sawyer, L., and Michael, J. Scanning electron Microscopy and X-Ray Microanalysis. Third Edition, Kluwer Academic/ Pleum Publishers, New York, 2003.

19. Jennings, Hamlin, Jeffrey J. Thomas. (2009). Materials of Cement Science Primer. Evanston, IL: Northwestern U Infrastructure Technology Institute.

20. Justnes, H. Lindgard, J. et al. 2016. Can Light Weight Aggregate (LWA) lead to Harmful ASR in the Field?. International Conference on Alkali Aggregate Reactions in Concrete, At Sao Paulo, Brazil, Volume: 15.

21. Kosmatka, Steven H., Panarese., William C. (1988) Design and Control of Concrete Mixtures. Skokie, IL: Portland Cement Association.

22. Kupresan, Darko. Heathman, J., Radonjic, M. (2013) Experimental Assessment of Casing Expansion as a Solution for MicroAnnular Ga Flow. Paper. SPE 168056 presented at IADC/SPE Drilling Conference, Fort Worth, Texas, 4-6 March.

23. Kutchko, B. et al. (2015) Field-Generated Foamed Cement: Initial Collection, Computed Tomography, and Analysis. National Energy Technology Laboratory.

24. Kutchko, B., Crandall, D., Spaulding, R., et al. (2016) A Look at Processes Impacting Foamed Cement. Society of Petroleum Engineers.

25. Lavrov, A. (2016) Lost Circulation: Mechanisms and Solutions. Amsterdam: Gulf Professional Is an Imprint of Elsevier.

26. Leemann, A., Lörtscher L., Et al. (2014) Mitigation of ASR by the Use of LiNO3—Characterization of the Reaction Products. Cement and Concrete Research 59: 73-86.

27. Lindgard, J. Andic-Cakir, O. Fernandes, I., …. Thomas, M. (2011). Alkali-silica Reactions (ASR): Literature review on parameters influencing laboratory performance testing. Cement and Concrete Research 42 (2012) 223-243.

28. M. Kawamura, N. Arano, T. Terashima, Composition of ASR gels and expansion of mortars, in: M. Cohen, S. Mindess, J. Skalny (Eds.), Materials Science of Concrete:

Special Volume—The Sidney Diamond Symposium, American Ceramic Society, Westerville, OH, 1998, pp. 261–276.

29. M. Regourd, H. Hornain, Microstructure of reaction products, in: P.E. Grattan-Bellew (Ed.), 7th International Conference on Alkali–Aggregate Reactions in Concrete, Ottawa, 1986, pp. 375–380.

30. M.A.T.M. Broekmans, Structural properties of quartz and their potential role for ASR, Mater. Charact. 53 (2004) 129–140.

31. Marzouk, H. Langdon, S. (2003). The effect of alkali-aggregate Reactivity on the mechanical properties of high and normal strength concrete. Cement and Concrete Composites 25 (2003) 549-556.

32. Mehdi Rashidi, Alvaro Paul, Jin-Yeon Kim, Laurence J. Jacobs, Kimberly E. Kurtis, Insights into delayed ettringite formation damage through acoustic nonlinearity, Cement and Concrete Research, Volume 95, 2017, Pages 1-8.

33. Mehta, P.K. P.j. Monteiro. (2006). Concrete: microstructure, properties, and material". McGraw-Hill.

34. Nelson, E. Guillot, D. (2006). Well Cementing Second Edition. Schlumberger. Sugar land, TX.

35. Pang, X., Maxson, J. K., Jimenez, W. C., Singh, J. P., & Morgan, R. G. (2016) Multiscale Characterization of Foamed Cement Using X-Ray Microcomputed Tomography. Society of Petroleum Engineers.

36. Peiliang Shen, Linnu Lu, Wei Chen, Fazhou Wang, Shuguang Hu, Efficiency of metakaolin in steam cured high strength concrete, Construction and Building Materials, Volume 152, 2017, Pages 357-366.

37. Ramirez, Jorge. (2016) Microparticle Compression Strength with Micro indentation. Nanovea.

38. Richard J. Davies, Sam Almond, Robert S. Ward, Robert B. Jackson, Charlotte Adams, Fred Worrall, Liam G. Herringshaw, Jon G. Gluyas, Mark A. Whitehead, Oil and gas wells and their integrity: Implications for shale and unconventional resource exploitation, In Marine and Petroleum Geology, Volume 56, 2014, Pages 239-254.

39. Robert D. Moser, Amal R. Jayapalan, Victor Y. Garas, Kimberly E. Kurtis, As-sessment of binary and ternary blends of metakaolin and Class C fly ash for alkali-silica reaction mitigation in concrete, Cement and Concrete Research, Volume 40, Issue 12, 2010, Pages 1664-1672

40. S. Diamond, N. Thaulow, A study of expansion due to alkali–silica reaction as conditioned by the grain size of the reactive aggregate, Cem. Concr. Res. 4 (1974) 591–607.

41. Sabin, F. (2005) Ultra-Lightweight Cement. CSI technologies. DOE final report.

42. Santra, Ashlk. Lou, Hougyn. (2016) Understanding Early Stage Cement Hydration at 400ºF in the presence of Inorganic Hollow Beads- an SEM Study. Halliburton.

43. Scherer, G.W., Valenza, J.J., and Simmons G. (2006) New Methods to Measure Liquid Permeability in Porous Materials. Cement and Concrete Research, Volume 37, pp. 386-397.

44. Schneider, José F., Nicole P. Hasparyk, Denise A. Silva, and Paulo J. M. Monteiro. (2010) Effect of Lithium Nitrate on the Alkali-Silica Reaction Gel. Journal of the American Ceramic Society 91.10: 3370-374.

45. Schultz, J. James, A. (2001) Hard and fast- the cement challenge. Middle East Reservoir Review.

46. Seidel, F. A., & Greene, T. G. (1985, January 1). Use of Expanding Cement Improves Bonding and Aids in Eliminating Annular Gas Migration in Hobbs Grayburg-San Andres Wells. Society of Petroleum Engineers.

47. Selecting Measures to Prevent Deleterious Alkali-Silica Reactions in Concrete. (2012) U.S. Department of transportation. Federal Highway Administration.

48. Snellings, R. Mertens, G. Elsen, J. (2012). Supplementary Cementitious Materials. Review in Mineralogy and Geochemistry. Vol. 74 pp. 211-278.

49. Swamy, R. N. 1992 "The Alkali-silica Reaction in Concrete". Glasgow: Blackie.

50. T. Knudsen, N. Thaulow, Quantitative microanalyses of alkali–silica gel in concrete, Cem. Concr. Res. 5 (1975) 443–454.

51. Tang, S.w., Y. Yao, C. Andrade, and Z.j. Li. (2015) Recent Durability Studies on Concrete Structure. Cement and Concrete Research 78: 143-54.

52. Taylor, W. (1997) Cement Chemistry. Thomas Telford, London, 2nd Ed.

53. Tremblay, C., M.a. Bérubé, B. Fournier, M.d. Thomas, and K.j. Folliard. (2010) Experimental Investigation of the Mechanisms by Which LiNO3 Is Effective against ASR. Cement and Concrete Research 40.4: 583-97.

54. Vidic, R.D., Brantley, S.L., Vandenbossche, J.M., Yoxtheimer, D., Abad, J.D., 2013. Impact of shale Gas development on regional water quality. Science 340, 6134.

55. Vignes, B., Aadnøy, B.S., 2010. Well-integrity issues offshore Norway. SPE 112535.

56. Zhang, Jie, Emily A. Weissinger, Sulapha Peethamparan, George W. Scherer. (2010) Early Hydration and Setting of Oil Well Cement. Cement and Concrete Research 40.7, 1023-033.

APPENDIX A: FULL HARDNESS AND YOUNG'S MODULUS DATA

Table A.1: All Hardness and Young's Modulus values for dry samples with lithium nitrate cured at room temperature

Hardness (Vickers)	Youngs Modulus (GPa)
5.81	3.29
6.14	3.45
4.38	3.64
6.07	4.21
6.85	4.66
5.25	3.29
5.08	4.2
4.82	3.91
7.09	4.18
5.33	3.8
5.8	3.2
6.92	4.59

Table A.2: All Hardness and Young's Modulus values for dry samples without lithium nitrate cured at room temperature

Hardness (Vickers)	Youngs Modulus (GPa)
9.15	4.7
8.42	3.89
11.28	5.62
7.76	5.02
6.43	4.89
11.89	5.31
11.52	6.69
6.97	3.01
8.49	4.34
5.49	3.85
7.74	4.78
8.07	4.61

Table A.3: All Hardness and Young's Modulus values for wet samples without lithium nitrate cured at room temperature

Hardness (Vickers)	Youngs Modulus (GPa)
5.51	5.07
6.37	6.01
6.18	10.63
5.45	6.4
6.35	6.66
6.01	5.16
6.45	7.38
5.93	7.95
4.96	5.44
5.26	8.16
5.62	6.35
5.87	5.17
6.2	6.8
5.68	6.32

Table A.4: All Hardness and Young's Modulus values for wet samples with lithium nitrate cured at room temperature

Hardness (Vickers)	Youngs Modulus (GPa)
3.8	3.61
3.59	3.42
3.89	3.38
4.8	3.87
3.59	3.14
4.28	3.18
3.79	2.27
1.21	2.28
3.48	2.29
4.29	4.54
4.56	4
4.18	4.73
3.9	4.01
4.23	3.7

Table A.5: All Hardness and Young's Modulus values for samples containing only microspheres cured at 70°C

Hardness(HV)	Elastic Modulus(GPa)
0.082247	5.202048
0.047708	4.354287
0.047044	3.273517
0.043927	4.992195
0.059684	8.021233
0.069719	5.689721
0.054357	4.139602
0.056458	4.695223
0.068953	5.325332
0.078053	6.012055
0.057168	4.311172
0.060787	5.289348
0.059557	4.49423
0.051285	7.13377
0.05763	5.378007
0.056048	5.185613
0.067201	10.99309
0.067069	5.194124
0.047792	5.386007
0.049368	5.608388
0.053412	6.82706
0.045439	4.279886
0.0503	6.895276
0.046592	6.399818
0.047182	5.754462
0.056502	5.776572
0.062191	6.79918
0.060593	6.798533
0.043557	4.872558
0.05123	5.44033

Table A.6: All Hardness and Young's Modulus values for samples containing microspheres and 2% lithium nitrate cured at 70°C

Hardness(HV)	Elastic Modulus(GPa)
0.048571	5.227666
0.043617	5.153232
0.038185	4.639826
0.044644	4.554465
0.043082	4.46802
0.046372	4.518296
0.047337	4.100683
0.065849	5.537067
0.045318	4.968249
0.037069	4.185772
0.064754	5.320602
0.041597	4.554202
0.051627	5.819282
0.048231	5.27932
0.063934	5.820747
0.040907	9.535896
0.034503	3.952893
0.049637	4.565068
0.044933	4.513351
0.059042	5.531892
0.047982	4.375151
0.048641	4.62314
0.037689	3.56215
0.037504	4.204872
0.044445	4.374275
0.070903	3.040105
0.033634	3.863028

Table A.6: All Hardness and Young's Modulus values for samples containing microspheres and 5% lithium nitrate cured at 70°C

Hardness(HV)	Elastic Modulus(GPa)
0.041535	5.416246
0.04776	3.171128
0.036808	5.484983
0.030779	4.752801
0.031693	4.670462
0.035925	1.251664
0.041409	4.212689
0.050306	5.2695
0.052995	4.596164
0.042312	3.23911
0.016389	2.185771
0.017927	2.068478
0.033109	2.944197
0.032506	2.680904
0.057162	2.714993
0.051214	3.48549
0.052851	3.78329
0.048243	3.681894
0.016033	1.521381
0.041555	5.4551
0.037402	5.510085
0.040528	2.861589
0.048819	1.60849
0.036283	5.055678
0.047137	4.348821
0.032455	4.425414
0.045853	3.460482
0.034768	4.204511
0.049566	5.054977

Table A.6: All Hardness and Young's Modulus values for samples containing microspheres and 8% metakaolin cured at 70°C

Hardness(HV)	Elastic Modulus(GPa)
3.532002789	3.608546523
3.876861283	4.005728226
4.14998496	4.246862247
4.061802361	4.12056106
3.23088756	3.464489848
5.369242732	4.635717249
4.335237106	4.406093409
4.340210933	4.457757494
4.623600898	4.216059325
3.750405822	4.110153139
3.394227898	4.517536196
4.657643157	4.52875578
3.884559813	4.467564668
12.32215611	7.577950035
4.736864342	4.815284019
3.649004426	4.577897761
6.179627944	6.232337388
4.200077888	4.073379515
5.641453781	4.798187694
3.834427645	3.695239079
4.619513774	4.983573986
4.133122929	4.649440916
6.189411648	5.638589989
4.832153974	4.770305877
7.710151566	6.718891299
10.2474664	9.408846283
11.1771136	8.744421059
9.720348675	8.340368909
5.149749526	5.941723862
4.929201032	4.831570103

Table A.6: All Hardness and Young's Modulus values for samples containing microspheres and 25% metakaolin at 70°C

Hardness(HV)	Elastic Modulus(GPa)
12.57786	8.488567
8.688786	7.716961
6.505904	4.658733
6.33874	4.344678
6.657248	4.687012
5.141916	4.933727
7.984652	4.171607
7.269217	5.021498
7.03539	6.118263
7.990078	4.642081
6.06026	5.133755
6.952668	6.489239
6.86961	6.119177
6.291656	5.604665
6.942026	8.325268
17.12935	9.299339
6.39772	5.975479
8.044406	7.299865
9.829876	6.490471
6.032128	5.001911
11.10414	4.644437
8.555883	2.300333
80.78148	8.92287
7.62168	2.308932
6.914698	1.850818
5.28153	3.223663
7.350336	2.874313
6.577614	4.486557
7.236179	2.806493
6.38187	2.414411

Table A.6: All Hardness and Young's Modulus values for samples containing microspheres and 15% Fly Ash cured at 70°C

Hardness(HV)	Elastic Modulus(GPa)
7.106188482	6.141569489
6.97564361	5.679570329
5.791840211	6.054031791
5.718484125	7.353695655
5.588472395	5.682257825
6.340332228	6.041811476
5.418300845	5.589447777
5.38831336	5.515257966
5.987638723	6.17601421
6.189960014	5.966155501
3.272065139	5.380579382
4.9459488	7.69007929
8.169065228	12.32122716
11.46535743	12.50914197
5.501922504	9.144344693
6.001338072	8.661180235
4.821666482	8.968812351
5.03517811	9.143881452
4.729352644	9.253702281
7.064304137	8.151858675
6.516374481	7.504093279
7.008845091	6.71383067
6.030500402	5.268138896
8.510102624	6.631621008
8.578321606	8.905808307
6.985827007	7.039488145
3.874364617	5.786100301
6.320834953	6.443339029
6.718114471	7.142854636
5.633919659	6.40892423

Table A.6: All Hardness and Young's Modulus values for samples containing microspheres and 30% fly ash cured at 70°C

Hardness(HV)	Elastic Modulus(GPa)
5.718499	3.105608
2.547877	1.993714
2.559784	1.840145
5.150375	2.671373
4.760451	0.885746
12.20662	6.98451
5.0357	2.770189
4.375714	2.507585
8.387039	7.925747
6.737622	9.112419
4.607072	6.588903
4.733497	6.875469
4.580772	7.657421
4.532776	6.82213
4.176746	7.582717
4.924528	5.594773
6.166333	9.574139
3.800517	6.996127
6.137309	5.257028
4.997801	4.771965
5.864098	4.44327
5.702392	4.24725
5.653603	4.723469
6.251019	3.959682
5.781167	6.569582
6.967772	4.819671
7.315673	5.739638
9.067647	5.96956

Table A.6: All Hardness and Young's Modulus values for samples containing microspheres and 15% silica flour cured at 70°C

Hardness(HV)	Elastic Modulus(GPa)
3.882051	3.377361
5.400572	5.485177
3.310534	3.438908
3.52674	4.033596
3.056053	3.417958
3.068423	2.739649
3.500051	2.915839
3.911631	3.769446
3.362505	3.72561
4.279858	4.812491
5.215811	4.223924
3.917803	4.909419
3.526006	4.465351
3.342617	4.620598
4.119439	3.940109
3.529334	4.730627
3.992457	4.751764
3.519686	4.421578
3.113814	3.981798
3.981402	2.535326
4.121487	3.259701
3.462326	2.760177
3.470182	3.083757
3.330567	2.949768
3.424494	1.885465
4.117738	3.063122
4.900884	3.947967
4.725087	3.642949
4.485851	3.406963

Table A.6: All Hardness and Young's Modulus values for samples containing microspheres and 30% silica flour cured at 70°C

Hardness(HV)	Elastic Modulus(GPa)
2.937165	4.78724
3.476075	3.764351
3.540767	6.085113
3.347192	5.677955
2.678913	4.858696
2.90385	4.163371
3.407556	8.506857
3.203747	7.758417
3.705067	8.749827
3.281581	6.443542
2.975558	2.540871
5.597512	2.842358
5.839924	2.999959
3.208361	3.267348
3.519625	0.874197
2.945778	3.285998
2.345847	2.961193
2.727201	3.18272
3.317893	3.776473
3.687275	3.86736
4.105106	2.958562
3.671334	2.449261
4.595739	4.212471
4.394451	4.506698
4.667079	3.899423
3.76537	3.813424
3.020235	3.300845
3.960847	3.687848
3.990112	4.044557
3.307244	4.323604

APPENDIX B: FULL POROSITY AND PERMEABILITY DATA

Table B.1: All sample data for porosity

	sample 1	sample 2	sample 3
No Add	44.86	44.4	45.18
2% LiNO3	46.34	46.788	41.15
5% LiNO3	45.75	47.76	46.4
15% FA	32.0614	30.65	27.18
30% FA	23.824	26.208	24.4381
8% MK	21.5278	19.9858	20.8826
25% MK	20.9032	19.5078	18.3514
15% SF	41.9515	40.5858	41.4736
30% SF	41.1541	42.5261	44.1926

Table B.2: All Sample data for permeability

	sample 1	sample 2	sample 3
No Add	5.51E-06		
2% LiNO3	2.77E-06	9.96E-06	
5% LiNO3	1.18E-06	3.43E-06	6.53E-06
15% FA	1.32E-06	8.70E-06	1.85E-06
30% FA	3.09E-06	7.46E-07	2.01E-07
8% MK	4.12E-07	5.86E-07	1.35E-06
25% MK	4.51E-07	9.45E-07	1.13E-07
15% SF	7.09E-07	2.55E-07	1.22E-06
30% SF	2.30E-06	1.30E-06	1.08E-07

APPENDIX C: MATERIALS USED IN EXPERIMENTS

B.1: Cement, Bentonite, Fly Ash, and Silica Flour

All cement used in these experiments were from the same batch of Haliburton Class H Premium Cement. Additionally, bentonite, class F fly ash, and silica flour came from Haliburton

B.2: Microspheres

All microspheres used in this study are 3M Glass Bubbles HGS19K46. These microspheres have a crush strength of 19000 psi and a density of .46 g/cc.

B.3 Metakaolin

Metakaolin used is PowerPozz from Advanced Cement Technologies

APPENDIX C: ADDITIONAL SEM IMAGES

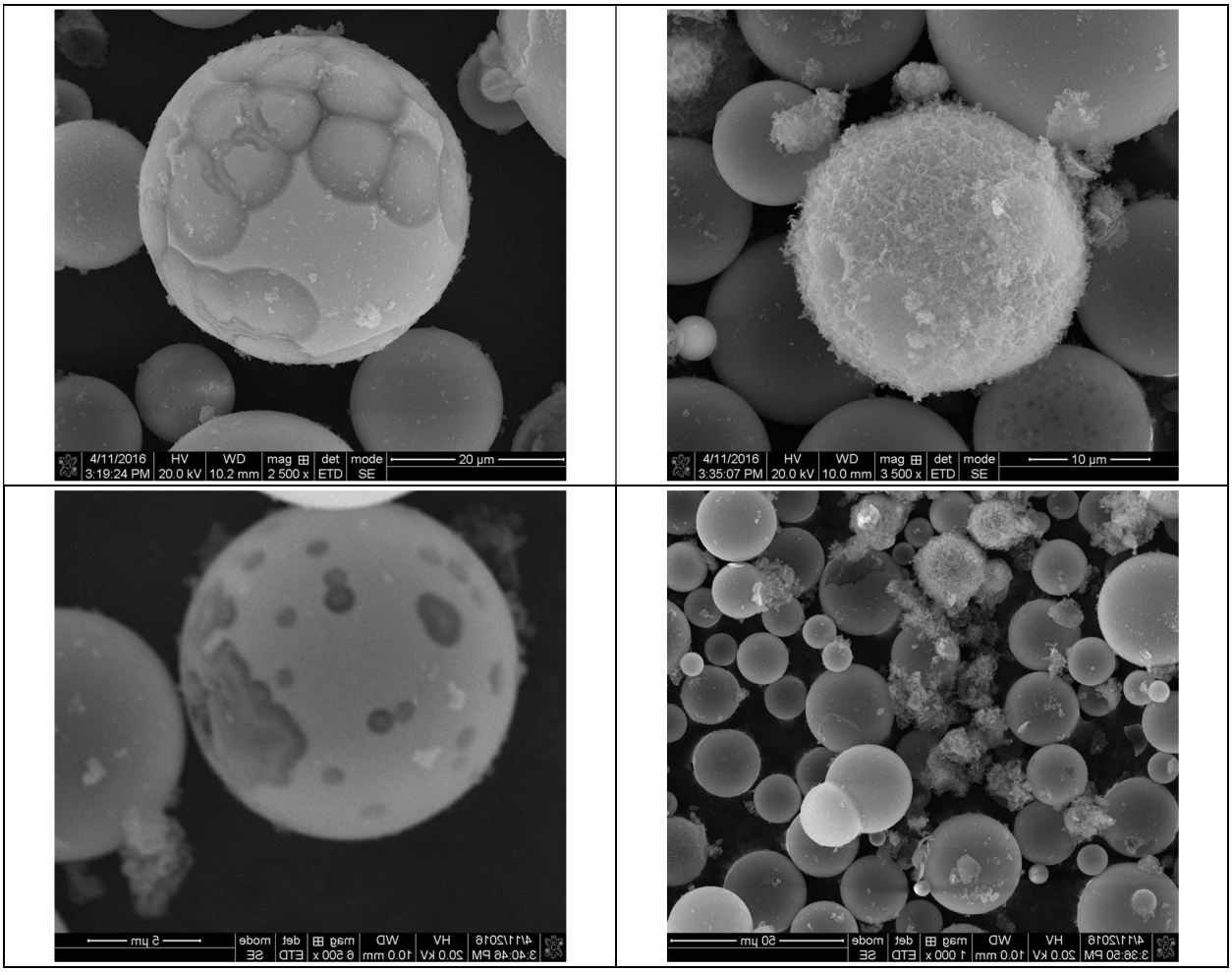

Figure C.1: Additional SEM images of microspheres from solution

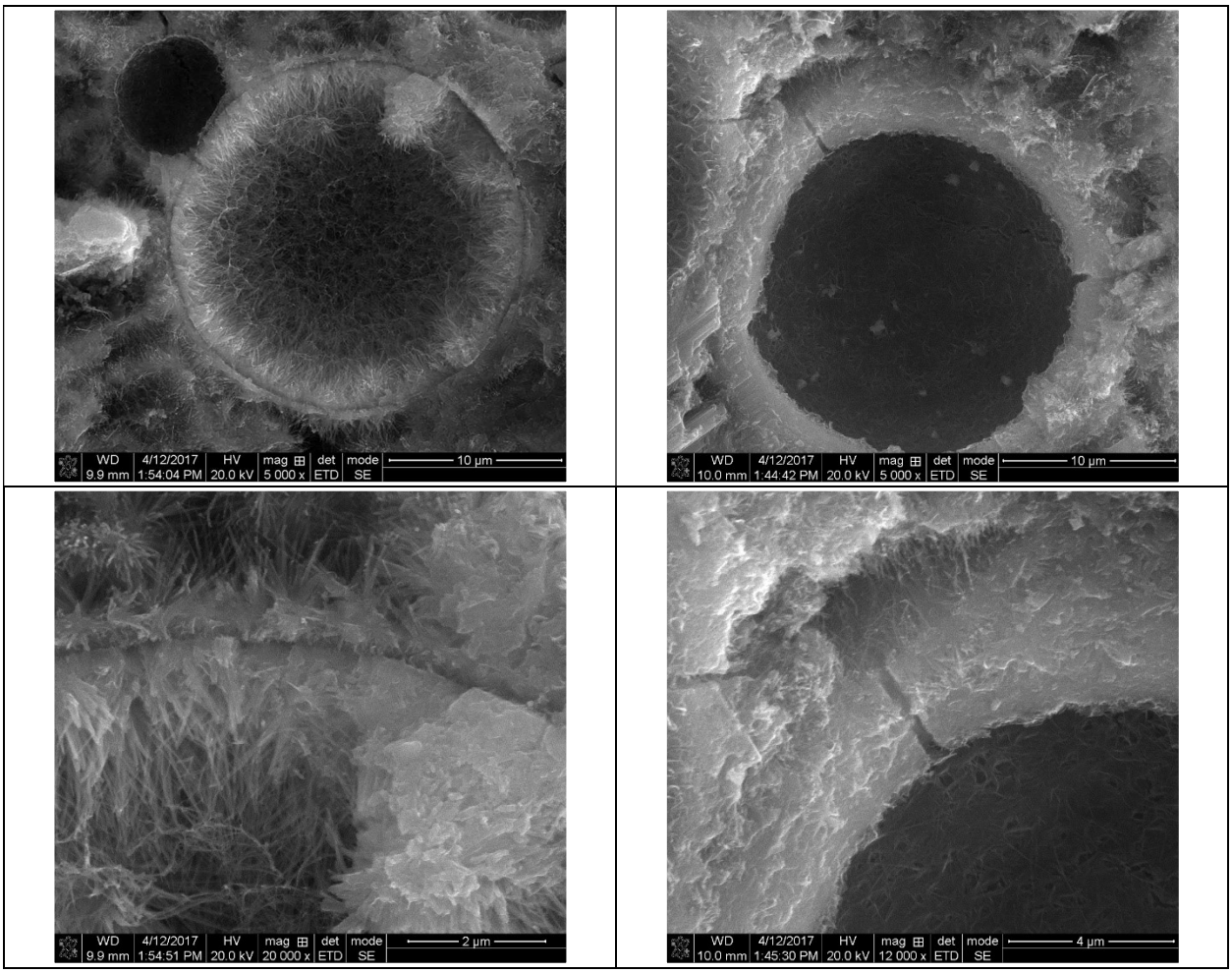

Figure C.2: Additional SEM images of microspheres in cement with no additives

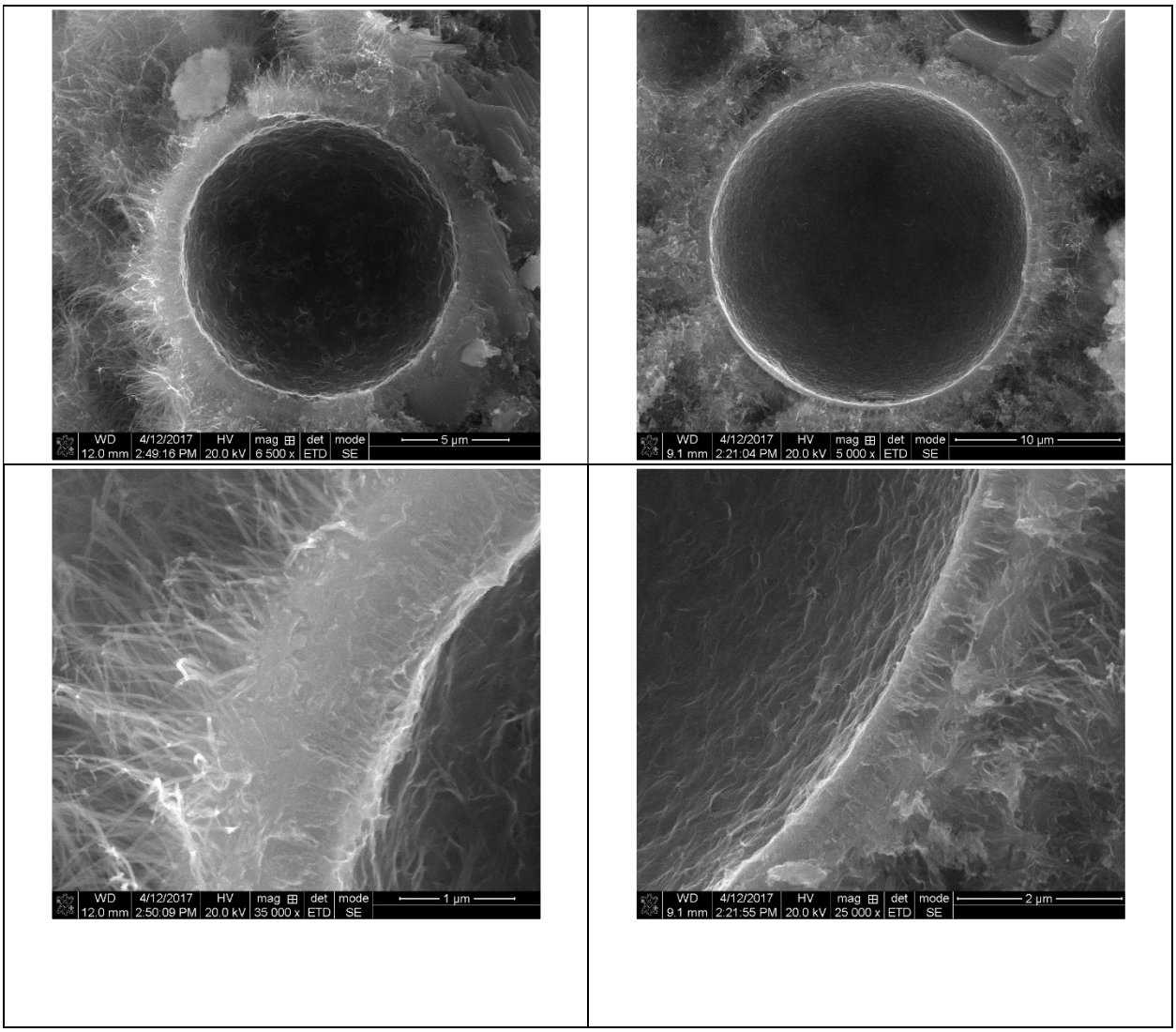

Figure C.3: Additional SEM images of microspheres in cement with lithium nitrate

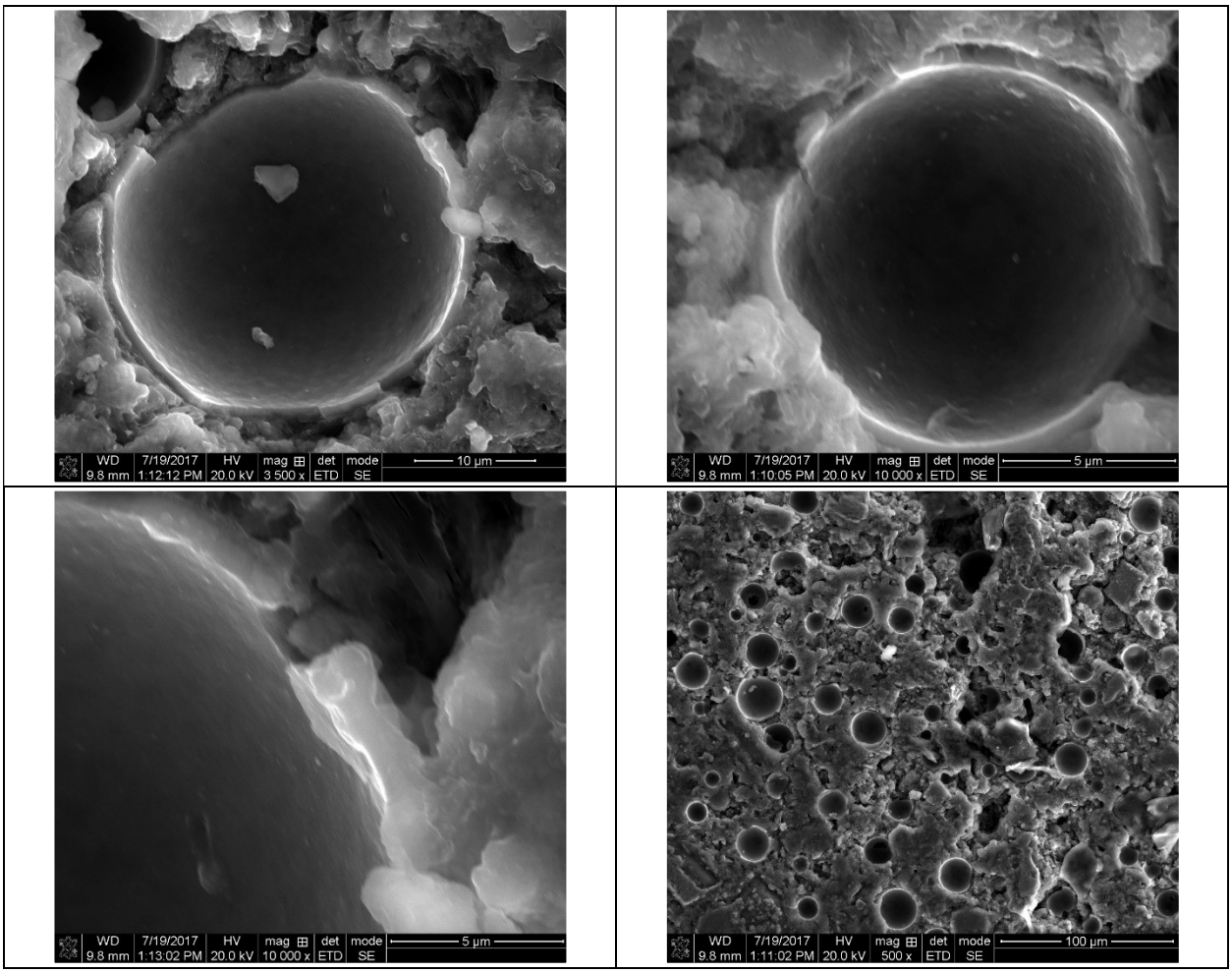

Figure C.4: Additional SEM images of microspheres in cement with metakaolin

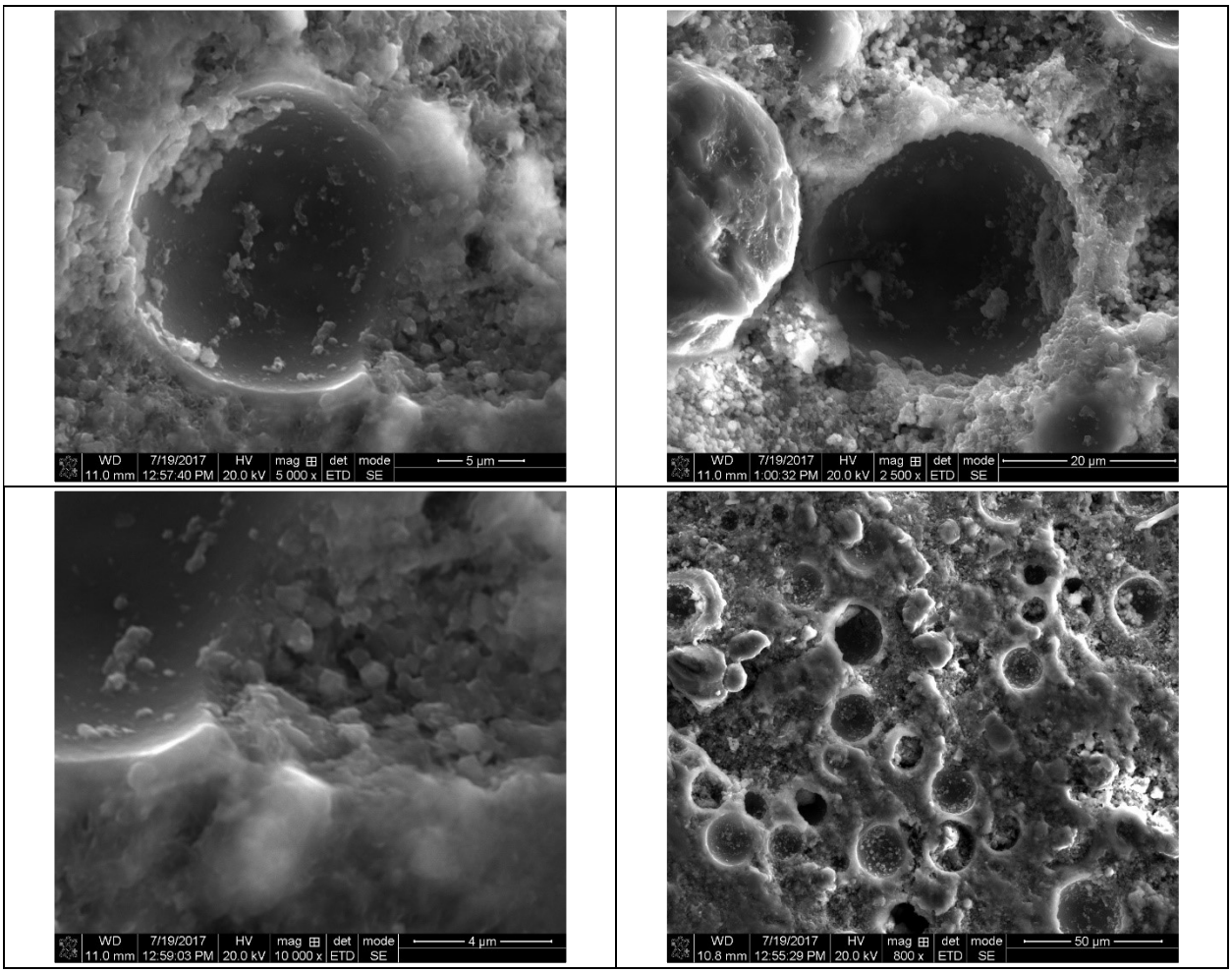

Figure C.5: Additional SEM images of microspheres in cement with metakaolin

APPENDIX D: SAMPLE PREPARATION

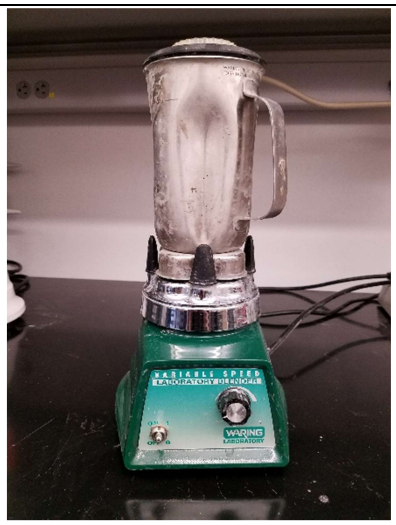	
Cement slurries were mixed in this 1 liter waring blender	After mixing slurries were poured into these lubricated 3”x1” cylindrical brass molds for 24 hours until being removed and put into alkaline bath solution
	
Core samples after being removed from the brass molds but before being put into solutions, notice uneven ends that need to be cut for experiments	Environmental chamber used to expose samples to high temperature. Displaying samples used in the expansion study. All samples were placed in sealed containers while in the environmental chamber

	
Barranca Diamond HP14 Slab saw used to cut samples down to 2” in length by cutting approximately .5” off each end for flat ends	Core samples after being cut down to 2” in length for experimentation

Figure C.1: Sample and experimental preparation

APPENDIX E: LIST OF PUBLICATIONS AND PROCEEDINGS

Albers, D. 2016. ***Durability of Glass Bubble Beads in Wellbore Cement Slurries: Impact of pH, Temperature, and Mixing.*** Presented at Deepwater Technical Symposium, New Orleans, Louisiana, August.

Albers, D. Radonjic, M. 2017. ***Prevention of Expansive Alakli- Silica Reaction (ASR) in Light-Weight Wellbore Cement.*** Paper OMAE2017-62015. Presented at the 36th International Conference on Ocean, Offshore & Artic Engineering, Trondheim, Norway, June 25-30.

Albers, D. (2017) ***Impact of Alkali-Silica Reaction (ASR) on Structural Integrity of Light-Weight Wellbore Cement.*** Paper SPE-189277-STU. Presented at the Society of Petroleum Engineers Annual Technical Conference and Exhibition, San Antonio, Texas, October 9-11.

VITA

Dylan Albers was born in St. Louis, Missouri in 1993 where he stayed until finishing high school in 2011. After graduating high school in St. Louis, he moved to Louisiana and started school at Louisiana State University (LSU). At LSU he completed his Bachelors of Science degree in Petroleum Engineering in 2015 and then began work on his Master's and plans to graduate in December 2017.